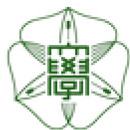
HOKKAIDO UNIVERSITY

| | |
|---|---|
| Title | Insulated gate and surface passivation structures for GaN-based power transistors |
| Author(s) | Yatabe, Zenji; Asubar, Joel T; Hashizume, Tamotsu |
| Citation | Journal of Physics D: Applied Physics, 49(39), 393001<br>https://doi.org/10.1088/0022-3727/49/39/393001 |
| Issue Date | 2016-09-07 |
| Doc URL | http://hdl.handle.net/2115/67317 |
| Rights(URL) | https://creativecommons.org/licenses/by/3.0/ |
| Type | article |
| File Information | JPD-2016.pdf |

Instructions for use

Hokkaido University Collection of Scholarly and Academic Papers : HUSCAP

OPEN ACCESS
IOP Publishing

Journal of Physics D: Applied Physics

J. Phys. D: Appl. Phys. 49 (2016) 393001 (19pp)

doi:10.1088/0022-3727/49/39/393001

## Topical Review

# Insulated gate and surface passivation structures for GaN-based power transistors

**Zenji Yatabe**[1], **Joel T Asubar**[2] and **Tamotsu Hashizume**[3]

[1] Priority Organization for Innovation and Excellence, Kumamoto University, Kumamoto 860-8555, Japan
[2] Graduate School of Engineering, University of Fukui, Fukui 910-8507, Japan
[3] Research Center for Integrated Quantum Electronics (RCIQE), Hokkaido University, Sapporo 060-0814, Japan

E-mail: yatabe@cs.kumamoto-u.ac.jp, joel@u-fukui.ac.jp and hashi@rciqe.hokudai.ac.jp

Received 9 September 2015, revised 16 June 2016
Accepted for publication 21 July 2016
Published 7 September 2016

**Abstract**

Recent years have witnessed GaN-based devices delivering their promise of unprecedented power and frequency levels and demonstrating their capability as an able replacement for Si-based devices. High-electron-mobility transistors (HEMTs), a key representative architecture of GaN-based devices, are well-suited for high-power and high frequency device applications, owing to highly desirable III-nitride physical properties. However, these devices are still hounded by issues not previously encountered in their more established Si- and GaAs-based devices counterparts. Metal–insulator–semiconductor (MIS) structures are usually employed with varying degrees of success in sidestepping the major problematic issues such as excessive leakage current and current instability. While different insulator materials have been applied to GaN-based transistors, the properties of insulator/III-N interfaces are still not fully understood. This is mainly due to the difficulty of characterizing insulator/AlGaN interfaces in a MIS HEMT because of the two resulting interfaces: insulator/AlGaN and AlGaN/GaN, making the potential modulation rather complicated. Although there have been many reports of low interface-trap densities in HEMT MIS capacitors, several papers have incorrectly evaluated their capacitance–voltage (*C*–*V*) characteristics. A HEMT MIS structure typically shows a 2-step *C*–*V* behavior. However, several groups reported *C*–*V* curves without the characteristic step at the forward bias regime, which is likely to the high-density states at the insulator/AlGaN interface impeding the potential control of the AlGaN surface by the gate bias. In this review paper, first we describe critical issues and problems including leakage current, current collapse and threshold voltage instability in AlGaN/GaN HEMTs. Then we present interface properties, focusing on interface states, of GaN MIS systems using oxides, nitrides and high-$\kappa$ dielectrics. Next, the properties of a variety of AlGaN/GaN MIS structures as well as different characterization methods, including our own photo-assisted *C*–*V* technique, essential for understanding and developing successful surface passivation and interface control schemes, are given in the subsequent section. Finally we highlight the important progress in GaN MIS interfaces that have recently pushed the frontier of nitride-based device technology.

Keywords: AlGaN, GaN, HEMT, MIS structure, *C*–*V*, interface state

(Some figures may appear in colour only in the online journal)

Original content from this work may be used under the terms of the Creative Commons Attribution 3.0 licence. Any further distribution of this work must maintain attribution to the author(s) and the title of the work, journal citation and DOI.

## 1. Introduction

GaN-based devices are considered to be the emerging front-runners to meet the ever growing demand for improved performance in terms of power, operation speed, and efficiency [1–4]. GaN's high critical electric field of over 3 MV $cm^{-1}$, which is a direct consequence of its wide bandgap of 3.4 eV, has permitted simultaneous realization of high breakdown voltages of over 1 kV and low specific on-resistances of about 5 mΩ $cm^2$ or less [5–15] in GaN-based high-electron mobility transistors (HEMTs). Using a combination of thick polycrystalline AlN passivation, via-holes structures, and field-plate schemes, Yanagihara *et al* have achieved a record off-state breakdown voltage value of 10.4 kV [16].

Meanwhile, electron saturation velocity as high as $2 \times 10^7$ cm $s^{-1}$ and high 2D electron gas (2DEG) density of over $1 \times 10^{13}$ $cm^{-2}$, originating from spontaneous and piezoelectric polarization fields as well as from large conduction band edge offset, make these devices also well-suited for high-power radio frequency (RF) applications. Downscaling of the gate length to sub-100 nm regime in conjunction with state-of the-art technologies has significantly increased the maximum current gain cutoff frequency ($f_T$) to over 200 GHz [17, 18]. Recently, Shinohara and co-workers [2, 19] have achieved ultrahigh-speed operation with record-high $f_T$ of 454 GHz with accompanying power gain cutoff frequency ($f_{max}$) of 444 GHz on a 20 nm gate HEMT. They have developed advanced technologies including an AlN/GaN/AlGaN double heterostructure, a side contact to the 2DEG and regrowth of $n^+$-layer in source/drain region, as shown in figure 1. This aggressive downscaling with a source-drain distance of 130 nm is again made feasible by the inherently high critical field of III–V nitride materials.

However, the very same unique material properties of GaN also led to some downside effects on device operation. A wide bandgap naturally leads to a wide variety of deeper traps, giving rise to the so-called 'current collapse'. Needless to say, the very same high critical electric field of GaN that has allowed unprecedented high voltage operation, also leads to a higher degree of charge injection and trapping, inducing more severe current collapse. Among the different approaches reported in literature to address the current collapse problem, surface passivation has become the standard technique because of its efficacy and simplicity [20, 21].

Another major issue is the 'normally-on' nature of GaN-based HEMTs. For reduced power consumption as well as failure protection, normally-off operation is highly preferred, in particular for a power switching devices. Obviously, normally-off devices requires a positive gate voltage to be turned on, which leads to exceedingly high leakage current levels in Schottky-gate devices. For normally-off operation of transistors, a metal–insulator–semiconductor (MIS) gate is absolutely necessary. Since the semiconductor/insulator interfacial quality significantly affects the transistor performance, a chemically stable MIS structure with low interface state densities should be developed for practical device applications.

A development of a stable MIS gate structure has been a challenging target in field-effect-transistors (FETs) using traditional III–V semiconductors such as GaAs, InP, InGaAs, etc. Among them, InGaAs MISFETs have gained much attraction due to their excellent carrier transport properties. In fact, the electron mobility in this system is more than 10 times higher than in silicon at a comparable sheet density, making the integration of the InGaAs MISFET on the Si platform highly desirable [22–24]. The MIS gate structure requires a dielectric free of trapped charge and other defects, few interfacial electronic states and high reliability. However, unlike Si, there have been no native oxides for III–V semiconductors that meet these requirements. In addition, various kinds of insulators/III–V structures prepared by a standard chemical vapor deposition (CVD) showed poor interface properties mainly arising from high-density interface states. The atomic layer deposition (ALD) technique opened the door for manufacturing III–V MOSFETs, because the ALD can provide relatively high-quality oxides/III–V interfaces. Ye *et al* [25] reported epoch-making performance from a GaAs MOSFET with an ALD $Al_2O_3$ gate, showing high $g_m$ and good RF characteristics. They later demonstrated significantly improved device performance on $Al_2O_3$-gate InGaAs MOSFETs with higher InAs compositions in the InGaAs channel [26]. Furthermore, very high effective channel mobilities over 4000 $cm^2$ $V^{-1}$ $s^{-1}$ were reported in ALD $Al_2O_3$-gate InGaAs MOSFETs [27, 28].

However, instability issues related to I–S interface states still remain in the InGaAs and GaAs MOSFETs [29]. In this relation, frequency dispersion at accumulation bias is a commonly observed feature in the experimental capacitance–voltage (*C–V*) characteristics of MOS structures using GaAs, InP and InGaAs [30–36], as shown in figure 2. To explain this instability behavior, the border trap (BT) model was proposed [37]. This model assumes defect levels inside the gate insulator, as shown in figure 3(a). In this case, BTs have long time constants as they interact with the conduction band electrons via tunneling, leading to large frequency dispersion even at accumulation bias [38, 39]. The disorder-induced gap state (DIGS) model [40, 41], as schematically shown in figure 3(b), can well explain frequency dispersion at accumulation bias. In this model, it is assumed that disordered region at the semiconductor surface includes defects, dangling bonds and lattice displacement (disorder in bond lengths and angles), thereby producing electronic states with density distributions in both energy and space. When interface states have space distribution, electron capture/emission processes also include tunneling effects. Recently, Galatage *et al* [36] reported a comparison of the BT and DIGS models by fitting both models to experimental data. Although both models suggested that frequency dispersion was caused by high-density electronic states within 0.8 nm from the crystalline semiconductor surface, they claimed that the experimental capacitance frequency dispersion in accumulation can be well explained by the DIGS model. This led them to conclude that frequency dispersion is indeed due primarily to disorder induced gap states in the semiconductor side. Moreover, since

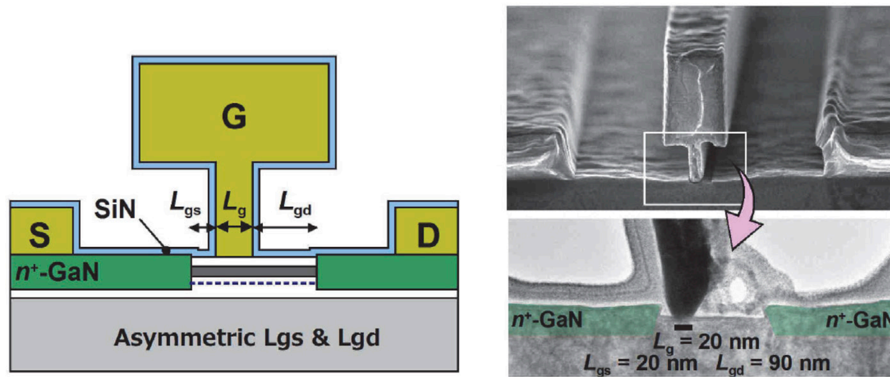


**Figure 1.** Schematic illustration and cross-sectional image of state-of-the-art GaN HEMT aggressively scaled for high frequency applications. (Reprinted with permission from [2], copyright 2013 IEEE.)

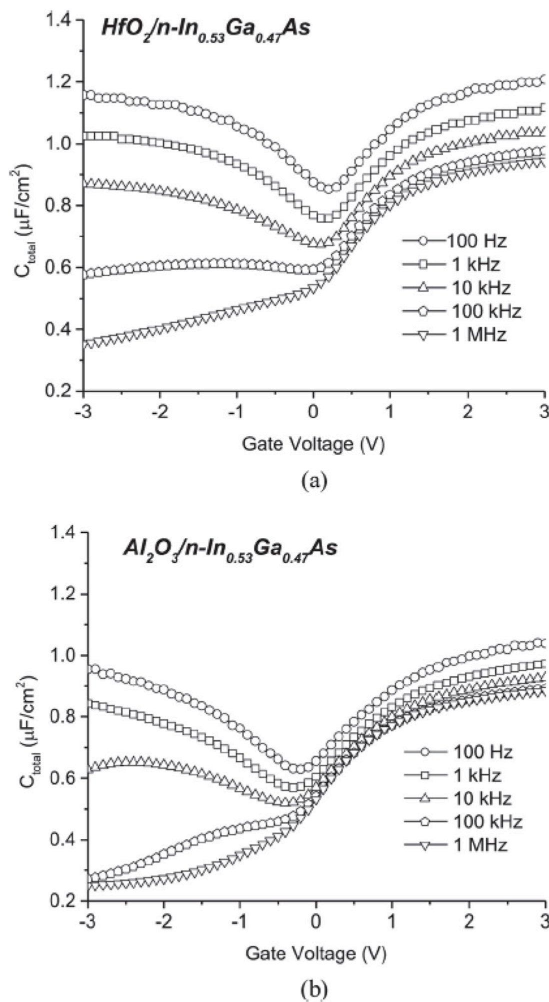


**Figure 2.** *C–V* characteristics as a function of frequency of (a) $HfO_2$ and (b) $Al_2O_3$ on *n*-InGaAs. (Reprinted from [36], copyright 2014 with permission from AIP Publishing.)

the *C–V* frequency dispersion in InGaAs MOS structures has been observed for a variety of dielectrics including $Al_2O_3$, $HfO_2$, $ZrO_2$, LaAlO, HfAlO, etc, it is unlikely that the same BT would have almost the same energy from the InGaAs conduction band edge can be consistently reproduced using different dielectric materials.

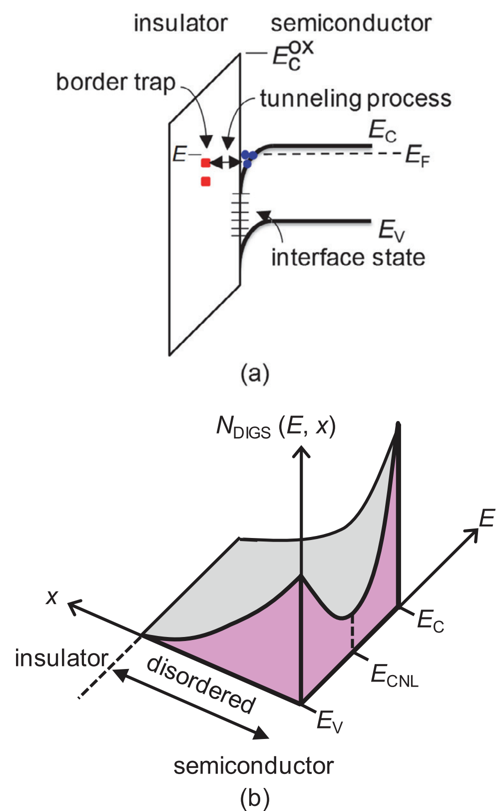


**Figure 3.** Schematic illustrations of (a) border trap (BT) model [37] and (b) disorder-induced gap state (DIGS) model [40, 41].

To develop a MIS gate applicable to practical devices, characterization of MIS interface properties have become of utmost importance for understanding the underlying physics required for circumventing problematic issues. Although different insulator materials have been used to GaN-based transistors including HEMTs, the resulting insulator/III-N interfacial properties are still not fully understood. This is partly due to the higher degree of complexity involved in these structures. In comparison with a conventional MIS structure having a single semiconductor layer, it is difficult to characterize the insulator/AlGaN interfaces in a MIS HEMT because it has two interfaces: insulator/AlGaN and AlGaN/GaN,

making the potential modulation rather complicated. In addition, the emission efficiency of electrons from the wide-gap interface states to the conduction band is very limited at room temperature (RT). For example, in the case of AlGaN with an Al composition of 30% ($E_G$ ~ 4.0 eV), the time constant for electron emission to the conduction band is estimated to be in the $10^{10}$–$10^{20}$ s range for near-midgap states at RT [42]. In this case, the charge condition of such deeper states cannot be changed by bias sweeping in a standard *C–V* measurement. Although there have been many reports of low interface-trap densities in HEMT MIS capacitors, several papers may have incorrectly evaluated their *C–V* characteristics. A HEMT MIS structure typically shows a 2-step *C–V* behavior [42]: one in the negative gate voltage regime that represents the total series capacitance of AlGaN and insulator layers, and the other in the positive gate voltage regime representing only the insulator capacitance. However, several groups reported *C–V* curves without the characteristic step at the forward bias regime. This is likely due to the high-density states at the insulator/AlGaN interface impeding the control of the gate over the AlGaN surface potential.

Eller *et al* [43] systematically reviewed surface and interface properties of GaN and AlGaN, including surface electronic/pinning models, reliability issues, surface treatment processes and dielectric passivation processes. Roccaforte *et al* [44] reported the review on dielectric technologies for SiC and GaN power devices, e.g. effects of interface states on channel mobility and stability of threshold voltage in SiC MOSFETs and improvement of device performance in GaN MOS HEMTs. In this article, we review insulated gate and surface passivation technologies for GaN-based MIS transistors including HEMT devices. First, we describe critical issues and problems including leakage current, current collapse and threshold voltage instability in AlGaN/GaN HEMTs. Then we present interface properties, focusing on interface states, of GaN MIS systems using oxides, nitrides and high-$\kappa$ dielectrics. Next, the properties of a variety of AlGaN/GaN MIS structures as well as different characterization methods, including our own photo-assisted *C–V* technique, essential for understanding and developing successful surface passivation and interface control schemes, are given in the subsequent section. Finally, we highlight the important progress in GaN MIS interfaces that have recently pushed the frontier of nitride-based device technology.

## 2. Instability issues in GaN-based HEMTs

### 2.1. Leakage currents in Schottky gates

Although significant progress has been achieved in GaN-based high-power/high-frequency electronic devices and ultraviolet photodetectors, surface-related problems still need an immediate solution. One of these issues is excessive leakage current through Schottky gate structures, which not only impedes device reliability but also degrades power efficiency and noise performance in such devices. In addition, del Alamo and Joh [45], Wu *et al* [46] and Meneghesso and co-workers [47–49] pointed out a strong correlation between the leakage current

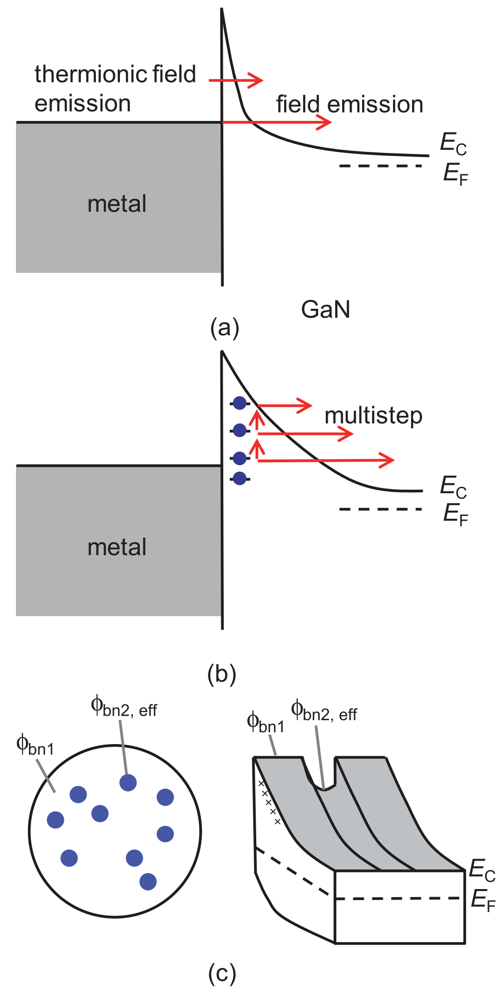


**Figure 4.** Schematic potential diagrams of (a) field emission (FE) and thermionic field emission processes and (b) trap-assisted tunneling model [53, 54]. (c) A patch model with different Schottky barrier heights [55].

via the Schottky gate edge on the drain side and electrical as well as structural degradation of AlGaN/GaN HEMTs. They indicated that a high electric field at the gate edge under off-bias condition induces electrically active defects in the AlGaN barrier due to inverse piezoelectric effect, providing a path for excess gate current.

To control reliability and degradation issues in Schottky gate GaN HENTs, we have to clarify the underlying leakage mechanism. Yu *et al* [50] and Miller *et al* [51, 52] discussed the leakage mechanism in GaN and AlGaN Schottky interfaces on the basis of the field-emission (FE) tunneling transport assuming a triangular Schottky potential, as shown in figure 4(a). However, unreasonably higher donor densities than the actual doping concentration were required in their calculation for reproduction of the experimental data. Thus, they speculated that the excessively high leakage current is due to some other processes such as defect-assisted tunneling or variable-range-hopping conduction through threading dislocations. Other groups also suggested the trap-assisted tunneling model (figure 4(b)) to explain the leakage mechanism in the reverse bias region [53, 54]. However, such models require an unlikely multi-step tunneling process or defect continuum

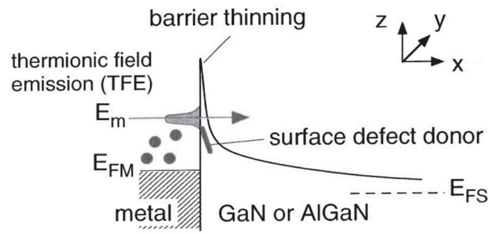


**Figure 5.** Schematic illustration of thin surface barrier (TSB) model. (Reprinted from [57], copyright 2004 with permission from AIP Publishing.)

with a wide energy band throughout a depletion region in the GaN or the AlGaN layer. As shown in figure 4(c), Sawada *et al* [55], meanwhile, suggested a surface patch model with different Schottky barrier heights to explain forward current characteristics.

Kotani *et al* [56] and Hashizume *et al* [57] proposed an entirely different model called the thin surface barrier (TSB) model for both forward and reverse current transport in GaN and AlGaN Schottky barriers. Here, it is assumed that the effective width of the Schottky barriers is reduced due to the presence of unintentional surface defect donors, and that thermionic field emission (TFE) or FE though the resultant TSB gives the major current leakage path in both forward and reverse directions, as shown in figure 5. They calculated *I–V–T* characteristics of GaN Schottky diodes with different density distributions of surface donors. Using the TSB model, they were able to explain the temperature dependences of measured *I–V* curves systematically. In particular, the TSB model reasonably reproduces various types of complicated *I–V–T* behavior in the reverse bias region. The most possible surface donors are nitrogen-vacancy ($V_N$) related defects [58, 59]. It is well known that Schottky contacts fabricated on the dry-etched GaN and AlGaN surfaces showed significant leakage currents [60, 61]. Indeed, plasma-assisted dry etching processes can induce a high density of $V_N$-related defects on the GaN and AlGaN surfaces [62, 63], enhancing TFE leakage transport via the $V_N$-related level. Recently, Hayashi *et al* [64] reported that a 2D simulation involving the TSB model well explained the gate-drain leakage characteristics of AlGaN/GaN HEMTs in a wide range of reverse bias voltage. They clarified that a leakage path between the gate and 2DEG at the gate edge on the drain side becomes dominant under higher drain-gate bias condition due to the concentration of high electric field at the gate edge.

Suda *et al* [65] precisely characterized Schottky diodes fabricated on free-standing *n*-GaN substrates with a low dislocation density of $2 \times 10^6$ cm$^{-2}$. They measured reverse *I–V* curves on the GaN diodes with different carrier densities, and showed that the measured curves excellently agree with the calculated curves on the basis of the TFE model without the need for fitting parameters (such as surface defect donors), as shown in figure 6. This indicates that Schottky diodes on the GaN layers with high crystalline quality (with low dislocation density) shows ideal *I–V* characteristics according to the simple TFE model. In comparison, high leakage currents with strong bias dependence and weak temperature dependence are still observed in Schottky gates fabricated

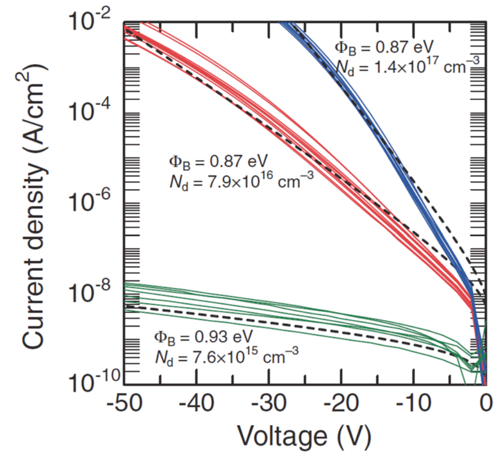


**Figure 6.** Reverse *I–V* curves of GaN Schottky diodes on GaN free-standing substrates with a low dislocation density of $2 \times 10^6$ cm$^{-2}$ and different donor concentration $N_d$. For all cases, measured curves agree with theoretical curves (broken lines) calculated using TFE model. (Reprinted with permission from [65], copyright 2010 by the Japan Society of Applied Physics.)

on AlGaN/GaN and InAlN/GaN structures [64, 66, 67], suggesting that the TFE transport enhanced by surface defect levels (TSB model) is dominant, which is related to relatively poor crystalline quality of thin AlGaN and InAlN barrier layers.

### 2.2. Current collapse

While GaN-based devices have recently reached the commercial product status, several problems still remain, and one such example of highest priority is the current collapse [68–70]. Current collapse is an important issue, because it may lead to a critically high ON-resistance ($R_{ON}$) immediately following device switching from OFF-state to ON-state. According to the widely accepted ‘virtual gate’ model [69], as shown in figure 7, a high OFF-state drain bias voltage induces electron trapping at the AlGaN surface states via a tunneling injection at the gate edge on the drain side. Subsequently, surface trapping depletes the underlying 2DEG and increases the drain resistance, leading to the increased dynamic $R_{ON}$, i.e. current collapse.

The current collapse (increase in $R_{ON}$) is strongly dependent on the drain voltage during the off-state stress [71, 72]. On the basis of the gate injection and surface-hopping model [70, 73], electron conduction via trap-to-trap hopping can be promoted with the application of increasing drain voltage. Consequently, this may lead to the widening of the ‘virtual gate’ from the gate edge until some further distance on the G–D access region. Using Kelvin probe force microscopy, Cardwell *et al* [74] demonstrated that trapping could extend as far as several hundred nanometers from the drain-side gate edge. After applying the off-state drain stress of 200 V to the AlGaN/GaN HEMT, Katsuno *et al* [75] observed electric field-induced second-harmonic signal within 2 $\mu$m from the gate edge on the drain side, corresponding to surface charging region. Tajima and Hashizume [76] and Nishiguchi *et al* [77] investigated current collapse behavior of AlGaN/GaN

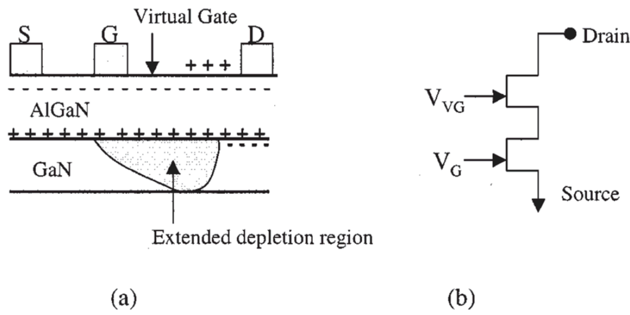


**Figure 7.** (a) Schematic illustration of the virtual gate model and (b) corresponding schematic representation of the device including the virtual gate. (Reprinted with permission from [69], copyright 2001 IEEE.)

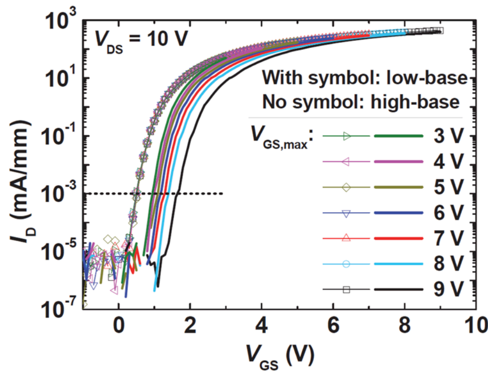


**Figure 8.** Dependence on maximum gate bias $V_{GS,max}$ of pulsed $I_D$–$V_{GS}$ transfer characteristics of the $Al_2O_3$/AlGaN/GaN MIS HEMT. (Reprinted from [96], copyright 2013. This material is reproduced with permission of John Wiley & Sons, Inc.)

HEMTs using dual-gate structure. They showed that the off-state gate stress induces 'virtual gates' along both sides of the gate edges expanding toward both the drain and source directions. They also found that off-stress induced surface charging region can extend as far as 0.5 $\mu$m from the gate edge toward the drain side.

Several groups pointed out that an acceptor-type bulk trap in the GaN layer is one of the candidate traps that induce current collapse in AlGaN/GaN HEMTs. Nakajima *et al* [78] demonstrated that a deep acceptor level is correlated with current collapse phenomena. However, their calculation result indicated that such deep acceptor with a relatively high density of 5 $\times$ $10^{16}$ $cm^{-3}$ caused only 10% reduction of drain current after an off-state bias stress. Recently, Faramehr *et al* [79] reported that the contribution of a bulk acceptor trap to off-state-induced current collapse was negligible in AlGaN/GaN HEMTs even when the GaN layer includes a bulk acceptor trap with a density of 2 $\times$ $10^{16}$ $cm^{-3}$. There have been no reports of epitaxial GaN layers including deep levels with densities higher than 5 $\times$ $10^{16}$ $cm^{-3}$ [80, 81]. In addition, surface passivation structure is effective in mitigating current collapse. These results indicate that off-state induced current collapse dominantly originates from the virtual gate effect caused by excess negative charges on the AlGaN surface (surface state charges) and/or in the AlGaN barrier layer.

Various approaches have been reported to control current collapse, such as the introduction of field-plate structures

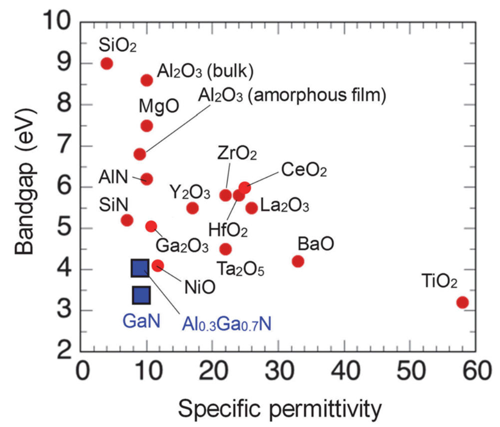


**Figure 9.** Energy gap versus relative permittivity for various insulators and (Al)GaN compounds.

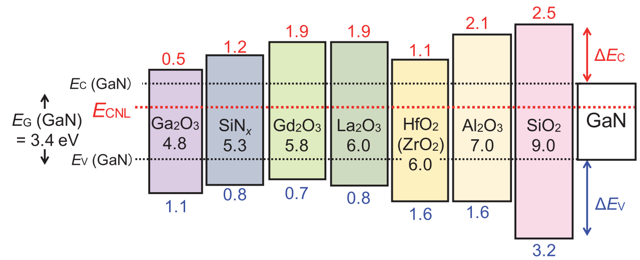


**Figure 10.** Band lineups at insulators/GaN interfaces calculated by Robertson and Falabretti [106].

[82–86] and employing high resistance nanowire channel structures [87, 88]. Surface passivation structures using dielectric films such as $SiO_2$, $SiN_x$, AlN, $Al_2O_3$ and others, are also very important for the realization of operation stability and reliability for various kinds of semiconductor devices. For III-N devices, in particular, it has been reported that the $SiN_x$-based passivation scheme is effective in mitigating current collapse due to a relatively low state density at the $SiN_x$/III-N interface [21, 89–91]. Green and co-workers [20] were the first to demonstrate the efficacy of the $SiN_x$ passivation of AlGaN/GaN HEMTs for reducing surface trapping effects, thus leading to increased output RF power. Derluyn *et al* have reported that the *in situ* MOCVD deposition of $SiN_x$ on the AlGaN surface significantly improved the DC performance of AlGaN/GaN HEMTs [92]. Meanwhile, epitaxial GaN cap layers have also been employed to modify device surface potential in order to decrease current dispersion [93–95]. While those methods have been demonstrated to be effective, current collapse still persists at high voltage switching stages even when using a combination of aforementioned schemes [85].

### *2.3. Threshold voltage ($V_{TH}$) fluctuation in AlGaN/GaN MIS HEMTs*

While keeping the merits of conventional Schottky-gate-based HEMTs, i.e. a high density of 2DEG at the AlGaN/GaN interface, high cutoff and maximum frequencies, and thermal and chemical stability of AlGaN and GaN, MIS HEMTs offer many advantages over Schottky-gate-based HEMTs, such as

**Table 1.** Experimentally obtained band offsets from GaN and AlGaN MIS structures reported in literatures.

| Structure | Deposition method | $E_G$ (eV) | $\delta E_V$ (eV) | $\delta E_C$ (eV) | Estimation method | Reference |
|---|---|---|---|---|---|---|
| $SiO_2$/GaN | JVD | — | 3.2 | 2.3 | F–N plot | [108] |
| | Plasma oxidation of Si | — | 2.0 | 3.6 | XPS | [109] |
| | PEALD | 8.9 | 3.2 | 2.3 | XPS | [110] |
| $SiN_x$/GaN | ECR-CVD | — | 0.7 | 0.8 | XPS | [21] |
| | Plasma nitridation of Si | — | −0.6 | 2.1 | XPS | [111] |
| $Al_2O_3$/GaN | ALD | 6.7 | 1.2 | 2.1 | F–N plot | [104] |
| | ALD | — | 1.2 | 2.1 | *C–V* | [101] |
| | PEALD | 6.7 | 2.1 | 1.2 | XPS | [110] |
| Sapphire/GaN | MBE(GaN) | — | 1.7 | 3.7 | XPS | [112] |
| $Ga_2O_3$/GaN | Anodic oxidation | — | 0.9 | 0.6 | P–F plot | [113] |
| | EB evaporation | — | 1.0 | 0.3 | XPS | [114] |
| $HfO_2$/GaN | Plasma oxidation of Hf | — | −0.1 | 2.5 | XPS | [115] |
| | ALD | — | 0.5 | 1.7 | XPS | [116] |
| | PEALD | 5.8 | 1.5 | 0.9 | XPS | [110] |
| $Cd_2O_3$/GaN | EB evaporation | 5.4 | 0.55 | 1.45 | XPS | [117] |
| $La_2O_3$/GaN | MBE | — | 0.63 | 1.47 | XPS | [118] |
| $SiN_x/Al_{0.3}Ga_{0.7}N$ | ECR-CVD | 4.9 | 0.1 | 0.7 | XPS | [21] |
| $Al_2O_3/Al_{0.3}Ga_{0.7}N$ | Plasma oxidation of Al | 7.0 | 0.8 | 2.1 | XPS | [21] |
| $Al_2O_3/Al_{0.25}Ga_{0.75}N$ | ALD | 6.9 | 1.2 | 1.8 | XPS | [119] |
| $HfO_2/Al_{0.25}Ga_{0.75}N$ | ALD | 5.9 | 0.9 | 1.1 | XPS | [119] |

lower gate leakage current, mitigation of current collapse, a wider range of allowable gate voltage sweep, and higher maximum drain current and output power. These features are crucial for applications in high-power and high-temperature electronics, particularly for realizing low on-resistance and normally-off high-power FETs.

Although various kinds of insulator materials have been applied to improve the performance of AlGaN/GaN MIS HEMTs, several problems remain unsolved. The most serious issue is the $V_{TH}$ instability. Several papers reported that different bias conditions induce varying degrees of $V_{TH}$ shifts in MIS HEMTs [96–98]. Lu *et al* [96] and Johnson *et al* [98] reported that a higher positive gate biasing of the MIS HEMTs induces larger $V_{TH}$ shift toward the forward bias direction. As shown in figure 8, Lu *et al* [96] reported from the pulsed $V_G$–$I_D$ measurement that higher gate-bias stress caused the larger $V_{TH}$ shift in their $Al_2O_3$-gate AlGaN/GaN HEMTs. A similar $V_{TH}$ fluctuation was also observed in $SiO_2$- or SiN-gate AlGaN/GaN HEMTs [99, 100]. Fixed charges in insulator films [101, 102], BTs in insulator films near the insulators/AlGaN interfaces [96, 99, 100] and interface states at the insulators/AlGaN interfaces are involved in the $V_{TH}$ shift mechanism. Ťapajna *et al* [97] discussed the effect of interface states on the $V_{TH}$ shift in $Al_2O_3$-gate AlGaN/GaN HEMTs. Many papers reported that high densities of electronic states still exist at the insulators/AlGaN interfaces. The charging state of the interface traps varies with the gate bias (surface potential), and deeper electronic states with long time constants for electron emission contribute to a slow $V_{TH}$ fluctuation.

Yang *et al* [103] demonstrated that surface nitridation of GaN/AlGaN/GaN structure using remote $N_2$ plasma is effective in improving the sub-threshold gate control and $V_{TH}$ stability of $Al_2O_3$-gate HEMTs. Hori *et al* [104] reported that $N_2O$ radical treatment can decrease interface states at the $Al_2O_3$/AlGaN interface, resulting in the improved stability of $V_{TH}$ even after applying an off-stress gate bias. Van Hove *et al* [105] utilized *in situ* $SiN_x$ as an interfacial control layer, and reported improved operation stability with a small $V_{TH}$ fluctuation in the $SiN_x/Al_2O_3$ gated AlGaN/GaN HEMTs. On the basis of a systematic characterization of interface states, further investigation is absolutely necessary to control electronic states at insulator/(Al)GaN interfaces for improved $V_{TH}$ stability of AlGaN/GaN MIS HEMTs.

## 3. Interface properties of (Al)GaN MIS structures

### *3.1. Band lineups at insulators-(Al)GaN structures*

For designing an MIS transistor or a surface-passivated transistor using a wide-gap semiconductor, it is important to understand the band lineup between the insulator and the semiconductor involved. Figure 9 shows the plot of energy gap versus specific permittivity for nitride semiconductors and insulators with a wide range of permittivity. It is a common knowledge that a higher value of dielectric constant leads to a higher value of transconductance $g_m$ in MIS transistors. In this regard, various types of gate stacks utilizing high-$\kappa$ insulators have been applied to GaN-based MIS transistors. In addition, a large band-offset energy is required at the insulator/(Al)GaN interface for the suppression of leakage current, in particular for device operation under forward bias condition. Among the insulators shown in figure 9, $Al_2O_3$ is one of the most attractive dielectric materials for power MIS devices because it combines all the desired properties such as large bandgap, relatively high dielectric constant, and high breakdown field (~10 MV $cm^{-1}$).

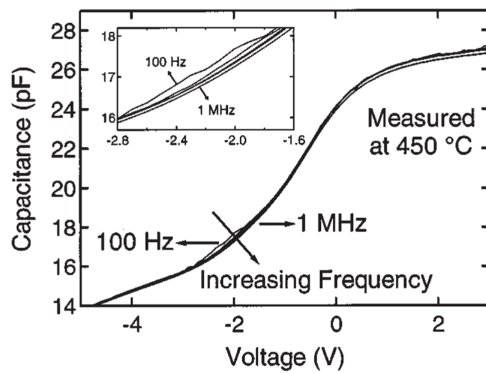


**Figure 11.** Frequency dispersion of *C–V* characteristics of $SiO_2$/$SiN_x$/$SiO_2$/*n*-GaN structure prepared by jet vapour deposition measured at 450 °C. Inset shows a blow-up of pertinent voltage region. (Reprinted with permission from [108], copyright 2001 IEEE.)

Figure 10 shows the band lineups between GaN and several insulators calculated by Robertson and Falabretti [106]. Based on the calculation of charge neutrality levels ($E_{CNL}$) as the reference energy, they have predicted the band alignments of GaN and relevant insulators. The $E_{CNL}$ is also used as the reference energy for the band lineups between semiconductor heterointerfaces [107]. All interfaces result in the type-I alignment. Table 1 summarizes the experimentally obtained band offsets from some GaN and AlGaN MIS structures reported in literatures [21, 101, 104, 108–119]. X-ray photoelectron spectroscopy analysis and leakage current characterization are often used to estimate the bandgap of an insulator and the band offset between insulator and semiconductor [21].

The calculated result indicates good standard for band offset at the insulator-semiconductor interface. Note that the bandgap of $Al_2O_3$ obtained experimentally from amorphous films [120, 121] ranges from 6.7 to 7.0 eV, which is lower than that of the bulk. Calculations predict that $Ga_2O_3$, $SiN_x$ and $HfO_2$ ($ZrO_2$) interfaces produce relatively low conduction-band barriers ($\Delta E_C$) in the conduction band, in good agreement with the experimental values. Although high-$\kappa$ dielectrics are very attractive to realize high $g_m$ in MIS transistors, relatively high leakage current may arise at forward bias when these insulators are used in the insulated gate structures. On the other hand, the resulting $\Delta E_C$ values from $Al_2O_3$ and $SiO_2$ are high enough to prevent excessive forward leakage current for MIS gate applications.

### 3.2. Oxide/(Al)GaN structures

During the early development stage of AlGaN/GaN HEMT technology, Khan and co-workers [122, 123] applied $SiO_2$ and $Si_3N_4$ to MIS gate structures to control gate leakage current and to improve gate-voltage swing capability. In this connection, interface properties of insulator/GaN structures have been accordingly investigated. Gaffey *et al* [108] reported a detailed characterization of interface properties of a $SiO_2$/$SiN_x$/$SiO_2$/*n*-GaN structure prepared by jet vapour deposition given in figure 11. From the conductance-frequency analysis, they obtained a state density of $5 \times 10^{10}$ $cm^{-2}$ $eV^{-1}$ at $E_C - 0.8$ eV with capture cross section of $2.4 \times 10^{17}$ $cm^2$ for the MIS sample fabricated using the optimum process condition. Matocha *et al* [124] and Kim *et al* [125] presented low state densities at the $SiO_2$/*n*-GaN interfaces prepared at high temperatures (830–900 °C). It was also found that high-temperature annealing process (around 900 °C) after the $SiO_2$ deposition was effective in decreasing the interface state density [126–129]. Kirkpatrick *et al* [130] and Takashima *et al* [131] reported that ALD-$SiO_2$ insulators prepared using 3-aminopropyltriethoxysilane or tris(dimethyl-amino) silane as Si sources were applicable to MOS gate structures. Kambayashi *et al* [132] demonstrated an $Al_2O_3$/$SiO_2$ bilayer gate structure achieving a field-effect mobility as high as 192 $cm^2$ $V^{-1}$ $s^{-1}$ in a recessed GaN channel structure by dry etching. Although $SiO_2$ film has a low permittivity as shown in figure 9, it remains attractive for MIS HEMT applications because of its large bandgap and chemical stability.

As mentioned in section 3.1, the $Al_2O_3$ dielectric material has a large bandgap, a relatively high dielectric constant, and a high breakdown field. In addition, there has been substantial progress in ALD technology, simplifying the application of $Al_2O_3$ to gate and passivation structures in GaN transistors [133, 134]. In fact, Ye *et al* [134] first demonstrated excellent electrical characteristics, such as low gate leakage current, high drain current, high $g_m$ and high channel mobility, in $Al_2O_3$-gate AlGaN/GaN HEMTs. The ALD process realized good $Al_2O_3$/*n*-GaN interface with a low state density of around $1 \times 10^{11}$ $cm^{-2}$ $eV^{-1}$ at $E_C - 0.8$ eV [135, 136]. When using $Al_2O_3$, however, special attention should be given to subsequent process temperature. From TEM investigations, Hori *et al* [135] observed that the as-deposited ALD-$Al_2O_3$ layer has an amorphous-phase structure and that the $Al_2O_3$/GaN interface is uniformly flat. However, annealing at 800 °C, a typical temperature for the formation of ohmic electrodes, generated a large number of microcrystallized regions in the $Al_2O_3$ layer, causing a marked increase in the leakage current of the $Al_2O_3$/GaN structure. Toyoda *et al* [137] also reported that annealing procedures at 800 °C resulted in the phase transformation of $Al_2O_3$ films from amorphous to crystalline. To address this issue, a surface protection layer is indispensable to avoid the chemical bond disorder on the (Al)GaN surface during the annealing process.

Esposto *et al* [101] and Son *et al* [102] inferred that fixed charges in $Al_2O_3$ films can shift flat-band voltages in the *C–V* curves of the $Al_2O_3$/*n*-GaN capacitors. The physical origin of the fixed charges, however, is still unresolved. Choi *et al* [138] theoretically predicted that the oxygen vacancies in $Al_2O_3$ introduce transition levels close to the conduction band edge of GaN, and they can act as BTs at the $Al_2O_3$/*n*-GaN interface. On the other hand, it is also likely that other kinds of defects such as the Al vacancy and interstitial act as fixed charges in $Al_2O_3$ [138]. As for reliability of the ALD $Al_2O_3$ layer, Kikuta *et al* [139] reported a time-to-breakdown ($t_{BD}$) value at 3 MV $cm^{-1}$ of more than 40 000 years at RT for an ALD-$Al_2O_3$ film. However, the $t_{BD}$ significantly decreased to $10^2$–$10^3$ s when temperature was raised to 250 °C.

The formation of a native oxide of AlGaN is rather appealing, because the oxidation process consumes the AlGaN

barrier layer, leading to the recessing of AlGaN and the subsequent local depletion of the 2DEG underneath the AlGaN oxide. On top of these, the native oxide of AlGaN itself can serve as a gate insulator for limiting the leakage current and for increasing the allowable gate voltage swing. These features are attractive for realizing nomally-off device operation. Medjdoub *et al* [140] have demonstrated a normally-off AlN/GaN HEMT with a native-oxide gate fabricated by selective dry oxidation of AlN at 900 °C. Greco *et al* [141] also reported that the annealing in $O_2$ at 900 °C produced crystalline native oxide at the AlGaN surface of the AlGaN/GaN structure. They showed that the oxidation process increased the lattice parameters as well as the mosaicity of the underlying semiconductor layers and significantly decreased the electron density at the AlGaN/GaN interface. However, aside from the fact that dry oxidation requires a high-temperature experimental condition it is very difficult for the dry oxidation to obtain an oxide of uniform thickness and a flat interface at the oxide/(Al)GaN interface [142–144]. One of the alternative techniques for the oxidation of AlGaN is by electrochemical process using low energies at RT in air. Mistele and co-workers [145] were the first to report AlGaN/GaN HEMTs with a native-oxide gate formed by the photoelectrochemical oxidation of AlGaN in a KOH-based solution. Eventually, Harada *et al* [146] demonstrated normally-off operation from AlGaN/GaN HEMTs with recessed oxide-gate structure formed by selective electrochemical oxidation. The recessed-oxide-gate HEMT with an oxide thickness of 20 nm showed good gate control of drain current with a threshold voltage of +1.2 V and a flat native oxide/AlGaN interface.

### 3.3. Nitrides/(Al)GaN structures

$SiN_x$ film is widely used for surface passivation of GaN-based transistors. Hashizume *et al* [21, 58] demonstrated that the $SiN_x$ deposition on $N_2$-plasma treated surfaces can produce a good $SiN_x$/*n*-GaN interface with a state density as low as $1 \times 10^{11}$ cm$^{-2}$ eV$^{-1}$ at $E_C - 0.8$ eV. The reason for the low interface state densities at the $SiN_x$/*n*-GaN interface is not yet fully understood. It is likely that nitrogen radicals generated during the $SiN_x$ deposition process control the formation of nitrogen-vacancy-related defects at the GaN surface [58, 59], leading to suppressed interface electronic states generation. In fact, the $N_2$-plasma surface treatment of the GaN and the AlGaN surface led to reduction of electronic state densities at the SiN/GaN interface [58] and improvement of device performance in SiN-passivated AlGaN/GaN HEMTs [147]. Green *et al* [20] were the first to apply $SiN_x$ passivation to the AlGaN/GaN HEMTs, and observed significant improvement of microwave output power from these devices as a consequence. $SiN_x$ gate was also used to AlGaN/GaN MIS HEMTs [122, 148, 149], from which significant reduction of current collapse was achieved. However, relatively high gate leakage current, in particular at forward bias, was observed in $SiN_x$-gate HEMTs [21, 148, 149], due to the small conduction band offset ($\Delta E_C$) between $SiN_x$ and (Al)GaN, as pointed out in the previous section.

The *in situ* deposition of $SiN_x$ by MOCVD is a promising process in the sense that it can be performed in the same growth chamber and in the same growth sequence as the rest of the layer stack [92]. During the final growth stage of the AlGaN/GaN structure by metal organic CVD, $SiN_x$ layer was *in situ* deposited using $NH_3$ and $SiH_4$ on the AlGaN surface at 1020 °C. Derluyn *et al* [92] obtained improved *I–V* characteristics from AlGaN/GaN MIS-HEMTs with a 3.5 nm thick *in situ* $SiN_x$ gate layer. The *in situ* process realized an oxide-free $SiN_x$/AlGaN interface [150]. From the high-resolution transmission electron microscopy (HR-TEM) analysis, Takizawa *et al* [151] reported that the *in situ* $SiN_x$ has a single crystalline structure. Moreover, Van Hove *et al* [105] have also demonstrated that an AlGaN/GaN MIS-HEMT with a stable threshold voltage and a low current collapse can be achieved using an *in situ* $SiN_x$/$Al_2O_3$ bilayer gate structure.

As shown in figure 9, the AlN film is also attractive as gate insulator and surface passivation layers. Hashizume *et al* [152] were the first to report relatively low densities of electronic states in the range of $10^{11}$ cm$^{-2}$ eV$^{-1}$ at the AlN/*n*-GaN interface. Tsurumi *et al* [153] demonstrated the fabrication of AlGaN/GaN HEMTs with a polycrystalline AlN surface passivation layer, taking advantage of the low thermal resistance of the AlN. They reported that the AlN-passivated HEMT showed a 30% higher drain current and a 66% lower $R_{ON}$ compared with those of HEMTs with SiN surface passivation. Recently, a monolayer-level ALD-AlN layer was used as an interfacial control layer for the $Al_2O_3$-gate AlGaN/GaN HEMTs [154].

### 3.4. High-κ dielectrics/(Al)GaN structures

High-κ insulators are attractive for achieving high $g_m$ in MIS transistors. Recently, relatively good *I–V* characteristics were reported from AlGaN/GaN HEMTs with high-κ gate insulators [155–159]. Deen *et al* [155] and Kikkawa *et al* [156] reported high $g_m$ values obtained from $Ta_2O_5$-gate AlGaN/GaN HEMTs. On the other hand, Yang *et al* [157] demonstrated $LaLuO_3$-gate AlGaN/GaN HEMTs showing good electrical performance such as high $g_m$, low gate leakage, small $V_{TH}$ fluctuation, and weak current collapse. Hatano *et al* [158] showed improved operation stability in AlGaN/GaN HEMTs with an $Al_2O_3$/$ZrO_2$ bilayer gate dielectric. Highly uniform epitaxially-grown NiO films prepared by MOCVD on AlGaN/GaN structure have also been reported [159]. However, the resulting NiO/AlGaN/GaN diode structure showed large leakage currents according to Poole–Frenkel mechanism, indicating the presence of electrical active defects in the MOCVD NiO [160]. Fiorenza *et al* [161] also reported epitaxial $CeO_2$ crystals grown by MOCVD on AlGaN/GaN structure. Although they observed relatively good *C–V* behavior, high values of leakage current were observed at forward bias for the MOS HEMT structure. Very recently, Chiu *et al* [162] reported $CeO_2$-gate AlGaN/GaN HEMTs fabricated using molecular beam deposition, and demonstrated good operation performance such as high $g_m$, low gate leakage, small sub-threshold swing (SS) and improved current collapse behavior. Meanwhile, Colón

and Shi [163] fabricated AlGaN/GaN MOS HEMTs using different high-$\kappa$ dielectrics such as $HfO_2$, $HfO_2/Al_2O_3$, $HfAlO_x$, and $HfSiO_x$ grown by ALD and compared their performance. Although they concluded that $HfAlO_x$ is the most promising insulating material, the $HfAlO_x$-gate HEMT still showed low $g_m$, pronounced current collapse and high interface state density. In addition, Deen *et al* [155] and Hayashi *et al* [164] reported severe $V_{TH}$ fluctuations from HEMTs with $HfO_2$-gate dielectric materials while Stoklas *et al* [165] described similar instability issues in HEMTs with $ZrO_2$-gate dielectric materials. Therefore, further investigation is necessary to gain better understanding of and improved performance from high-$\kappa$ insulators/(Al)GaN interfaces.

### 3.5. Effects of pre-deposition process and post-deposition annealing on MIS interface properties

Eller *et al* [43] reviewed surface processing of GaN such as wet chemical treatments, vacuum-annealing processes, gas annealing processes and ion/plasma treatments in detail. We here focus on surface treatment and post-deposition annealing processes that are effective in improving GaN MIS interface properties. Hossain *et al* [166] investigated wet treatments in solutions using $H_2O_2$:$H_2SO_4$ (piranha), $(NH_4)_2S$, and 30% HF, and showed that the smallest flat-band voltage shift for the $Al_2O_3$/*n*-GaN sample was achieved by the $H_2O_2$:$H_2SO_4$ treatment. However, the MOS samples after three processes showed almost the same values of $D_{it}$ of 1–3 $\times$ $10^{12}$ $cm^{-2}$ $eV^{-1}$. On the other hand, Chakroun *et al* [167] evaluated the *C*–*V* characteristics of $SiO_2$/*n*-GaN structures with pre-treatments by KOH, HCl, $NH_4OH$ and HF solutions. They reported that the treatment in KOH and HCl solutions resulted in the best RT *C*–*V* characteristics close to the calculated curve. However, even in this sample, a hysteretic behavior was observed with gate voltage sweeping between −3 and 3 V.

The H-plasma is often used to reduce native oxides and contaminants at the GaN surface. The H-plasma process, however, may simultaneously cause a chemical reaction with GaN and AlGaN surfaces to form volatile $NH_x$ groups, resulting in the formation of N-vacancy related defects and the degradation of GaN MIS interface properties [58, 59]. As described in section 3.3, on the other hand, the N-plasma treatment is effective in reducing $D_{it}$ in $SiN_x$/GaN interfaces, probably due to subdued formation of N-vacancy related defects as well as due to a cleaning effect on the GaN surface [59]. Chen *et al* [168] reported that a combination of $NH_3$ and $N_2$ plasma treatments before the deposition of $Al_2O_3$ by ALD significantly improved the AlGaN/GaN MOS HEMT performance due to the reduction of state densities at the $Al_2O_3$/AlGaN interface. They demonstrated that the $NH_3$ plasma treatment removes native oxides and the subsequent $N_2$-plasma process produces N-terminated AlGaN surface with compensation of N-vacancy related defects.

A post-deposition annealing in $N_2$ is generally used for the stabilization of GaN MIS interface properties, probably due to relaxation of dangling bonds and/or point defects at the GaN surface (insulator/GaN interface) during the annealing process. As mentioned in section 3.2, a high-temperature annealing (~900 °C) was effective in achieving good $SiO_2$/GaN interfaces with relatively low state densities [126–129]. On the other hand, the annealing temperature for the $Al_2O_3$/GaN structure is limited below 700 °C due to the phase transformation of the $Al_2O_3$ film from amorphous to crystalline. Winzer *et al* [169] recently reported that annealing at 500 °C in $O_2$ is more efficient for decreasing interface states of the $Al_2O_3$/GaN structure than annealing at the same temperature in $N_2$. Long *et al* [170] and Winzer *et al* [169] demonstrated that the annealing process at 400–500 °C using $H_2/N_2$ forming gas was promising to passivate interface states at the $Al_2O_3$/GaN interface, correlating the passivation effect with the incorporation of H atoms at the interface. However, it was found that the forming gas annealing drastically increased leakage currents of the $Al_2O_3$/GaN structure [169].

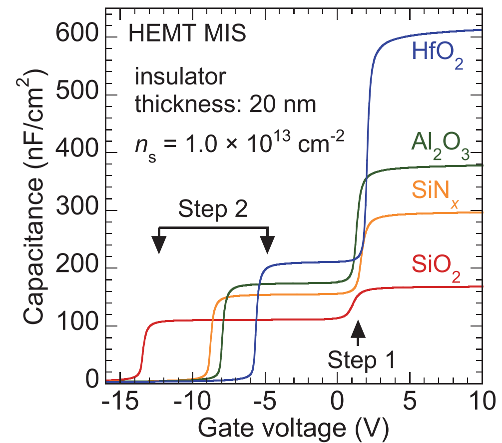


**Figure 12.** Calculated MIS *C*–*V* curves neglecting interface state density (ideal curves) for various insulators. (Reprinted with permission from [175], copyright 2014 by the Japan Society of Applied Physics.)

## 4. Characterization of electronic states at insulator/(Al)GaN interfaces using HEMT MOS diodes

### 4.1. Interpretation of HEMT MIS C–V characteristics

For practical device applications, in-depth understanding of insulator/AlGaN or insulator/InAlN interfaces using HEMT MIS structures is a key requirement. In this regard, precise interpretation of measured *C*–*V* characteristics from HEMT MIS structures is necessary. Although there have been many reports of low interface-trap densities in HEMT MIS capacitors, several papers have incorrectly evaluated their *C*–*V* characteristics, underestimating the actual interface state density for wide-gap semiconductors. A HEMT MIS structure typically shows a two-step *C*–*V* behavior [42]. However, numerous reports showed *C*–*V* curves without the characteristics step at the forward bias regime. When the gate voltage sweeping is confined within the reverse bias region, the resulting *C*–*V* curve often gives rise to misleadingly low density of electronic states at the insulator/AlGaN interfaces [171–173].

To interpret the typical two-step *C*–*V* behavior, Miczek *et al* [174] developed a calculation tool using a numerical solver of the Poisson equation based on the 1D Gummel

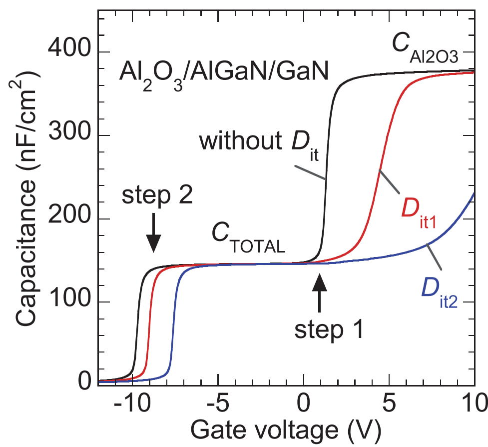


**Figure 13.** Calculated $C$–$V$ curves of 20 nm-$Al_2O_3$/AlGaN/GaN structure, taking into account the effect of interface electronic states. (Reprinted with permission from [175], copyright 2014 by the Japan Society of Applied Physics.)

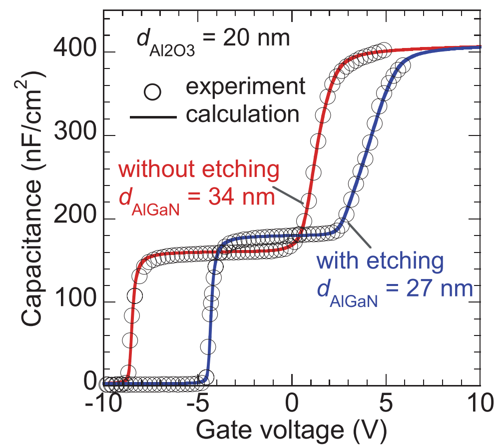


**Figure 14.** Comparison between calculated and experimental $C$–$V$ curves of $Al_2O_3$/AlGaN/GaN structure with and without the ICP dry etching of AlGaN surface. (Reprinted with permission from [175], copyright 2014 by the Japan Society of Applied Physics.)

algorithm, taking into account the fixed charge at the AlGaN/GaN interface originating from spontaneous and piezoelectric polarization as well as the charge in the electronic states at the insulator/AlGaN interface. Figure 12 shows an example of calculated MIS $C$–$V$ curves neglecting interface state density (ideal curves) for various insulators [175]. The characteristic two-step behavior is reproduced in the calculations. To evaluate the effects of interface states on the $C$–$V$ characteristics, Mizue at al [42]. and Yatabe *et al* [175] carried out calculations for the $Al_2O_3$/AlGaN/GaN structure, taking into account state density distribution ($D_{it}(E)$) consisting of acceptor- and donor-like states separated by the charge neutrality level $E_{CNL}$ [106, 174, 176, 177]. They used an electron emission time constant from interface states to the conduction band, evaluated using Shockley–Read–Hall (SRH) statistics, to identify the energy range of the interface states responsible for the observed $C$–$V$ behavior [178]. At an insulator-semiconductor interface, the crystalline periodicity of the semiconductor is terminated. In addition, disorder in atomic-bond arrangement can be induced at the semiconductor surface. In this case, separation of conduction and valence bands is insufficient, resulting in the penetration of bonding and anti-bonding states into the forbidden band (bandgap) from the valence and conduction bands, respectively [176, 179]. Therefore, the charging character of interface states also reflects those of the valence and conduction bands [176]. Namely, a negative charge appears in the conduction band if a state is occupied by an electron (acceptor-like character), and valence band state is positively charged when being unoccupied (donor-like character). Thus, it can be assumed that the interface state continuum consists of a mixture of acceptor-like and donor-like states, and their branch point act as the $E_{CNL}$. This model is often used as a density distribution of interface states [43, 180, 181].

An example of the calculated $C$–$V$ curves for the $Al_2O_3$/AlGaN/GaN structure is shown in figure 13 [175]. In the forward bias region, the $C$–$V$ slope drastically decreases with increasing interface state density. In this bias regime, the nearly flat potential of the AlGaN layer can lead to electron transfer from the AlGaN/GaN interface to $Al_2O_3$/AlGaN interface. Simultaneously, electron trapping at the $Al_2O_3$/AlGaN interface states is highly probable. The occupied acceptor-type states produce excess negative charges, which screen the applied gate electric field, suppressing the potential modulation of the AlGaN layer. This causes the stretch out of the $C$–$V$ curve in the forward bias regime, as seen in a standard MOS diode. If an insulator-AlGaN structure includes very high interface state densities, then the step 1 will not be observed even with high forward bias applied [182, 183]. On the other hand, at around the threshold bias (step 2), the Fermi level ($E_F$) is located far below the valence band maximum of AlGaN at the $Al_2O_3$/AlGaN interface. This makes electron occupation of interface states no longer a function of the gate bias [42, 175], leading to the absence of stretch-out behavior in the $C$–$V$ curve. In addition, the SRH statistics predicts very long time constants of electron emission from deep states to conduction band. Due to the associated long emission time constants, electrons captured in deep-lying acceptor-like traps remain trapped and act as negatively fixed charges at RT, even when a large negative bias is applied to the gate electrode. This leads to the parallel $C$–$V$ shift ($V_{TH}$ shift) at step 2 toward the positive bias direction with respect to the ideal $C$–$V$ curve, as evident in figure 13.

### 4.2. $D_{it}(E)$ estimation at insulator/(Al)GaN interface

By fitting the calculation results to the experimental $C$–$V$ curves, Yatabe *et al* [175] reported determination of $D_{it}(E)$ at $Al_2O_3$/AlGaN interfaces in HEMT MOS structures. Figure 14 shows the comparison between the calculated and experimental $C$–$V$ curves of the $Al_2O_3$/AlGaN/GaN structure with and without the inductively coupled plasma (ICP) dry etching of the AlGaN surface. To evaluate near-midgap electronic states at insulator/AlGaN interfaces at RT, Mizue *et al* [42] have developed a photo-assisted $C$–$V$ method using monochromatic lights with photon energies less than the bandgap of the AlGaN. The basic concept of photo-ionization effects of interface states under a monochromatic light with energy less that the bandgap of AlGaN is schematically shown in

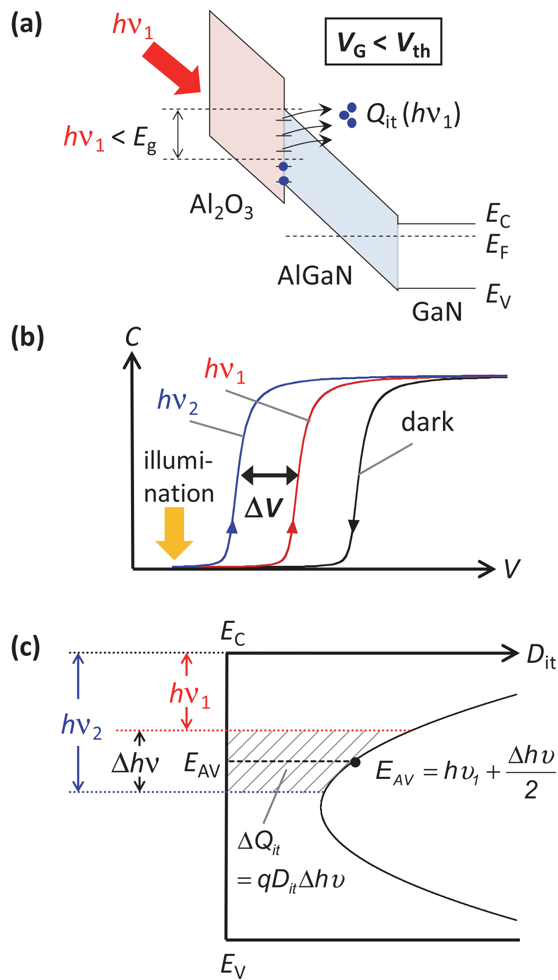


**Figure 15.** Schematic illustration of (a) photo-assisted electron emission at the $Al_2O_3$/AlGaN interface, (b) photo-assisted *C*–*V* characteristics and (c) interface state charge and energy range corresponding to the voltage shift, $\Delta V$, in photo-assisted *C*–*V* curves. (Reprinted with permission from [175], copyright 2014 by the Japan Society of Applied Physics.)

figure 15. In this method, the first step is application of a high enough forward gate voltage ($V_G$) to observe the insulator capacitance under dark condition to the HEMT MOS structures. At this state, almost all of interface traps are filled with electrons under a nearly flat band condition. Then, the gate bias is swept toward a value more negative than the $V_{TH}$, where a monochromatic light with photon energy of $h\nu_1$ is illuminated to the sample surface. Consequently, this effectively induces photo-assisted electron emission from the interface states within the energy range corresponding to the photon energy range, as schematically shown in figure 15. The subsequent $V_G$ sweeping after switching the light off results in the parallel *C*–*V* curve shift toward the reverse bias direction, corresponding to the change in the interface state charge $Q_{it}$ ($h\nu_1$), because the ionized state act as a fixed charge at a bias near $V_{TH}$. Using different photon energies, a systematic *C*–*V* shift according to the photon energy can be observed, as shown in figure 15. The voltage shift difference ($\Delta V$) between two photon energies corresponds to the interface charge difference, $\Delta Q_{it}$, in the energy range $\Delta h\nu$. The

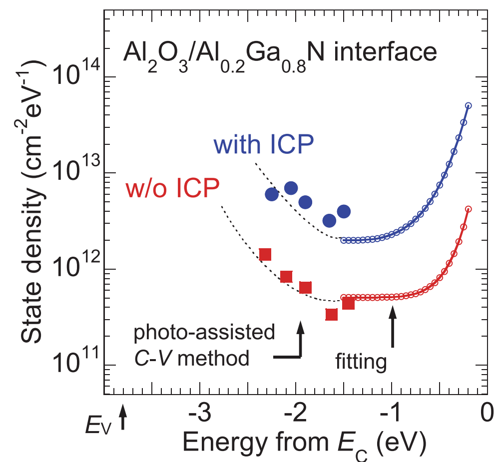


**Figure 16.** Interface states density distributions at the $Al_2O_3$/AlGaN interface determined by combination of photo-assisted *C*–*V* method and *C*–*V* fitting analysis. (Reprinted with permission from [175], copyright 2014 by the Japan Society of Applied Physics.)

state density can be simply estimated using the observed $\Delta V$ as given by the following equation [42]:

$$D_{it}(E = E_{AV}) = \frac{C_{TOTAL}\Delta V}{q\Delta h\nu}, \quad (1)$$

where $C_{TOTAL}$ is the total capacitance of insulator and AlGaN while $E_{AV}$ is the average interface energy.

Mizue *et al* [42] and Yatabe *et al* [175] reported systematic and parallel *C*–*V* shifts toward the reverse bias direction with increasing photon energy. Ozaki *et al* [184] also observed a similar parallel *C*–*V* shift in an ALD-$Al_2O_3$/*n*-GaN/AlGaN/GaN structure. These results indicate that the interface states near midgap or at deeper energies indeed act as fixed charges in this bias range. On the other hand, some groups have reported photo-assisted *C*–*V* characterization of MIS structures using a light source with photon energies larger than the GaN bandgap [185, 186]. In this case, holes are generated and accumulated at insulator/AlGaN and AlGaN/GaN interfaces. In addition, interaction of holes with the interface states especially at reverse bias has to be considered. This makes the charge dynamics in HEMT MIS structures complicated and the evaluation of interface state very difficult. Recently, Matys *et al* [187, 188] proposed a simulation method for the photo-assisted *C*–*V* characteristics, taking into account the electron-hole generation and the recombination processes as well as the hole capture process at the interface states. Comparing their calculation results to the experimental data, they were able to estimate the state density distribution at the $Al_2O_3$/AlGaN interface near the valance-band maximum of AlGaN.

Using the combination of the numerical fitting of *C*–*V* curves and the photo-assisted *C*–*V* method, for the first time, Yatabe *et al* [175] estimated the state density distribution of the $Al_2O_3$/AlGaN interfaces with and without the ICP dry etching of the AlGaN surface, as shown in figure 16. The sample without the ICP etching of AlGaN showed state densities of around $1 \times 10^{12}$ cm$^{-2}$ eV$^{-1}$ or less near the midgap.

On the other hand, much higher state densities were obtained at the $Al_2O_3$/ICP-etched AlGaN interface. TEM observations revealing the surface chemistry of AlGaN during the ICP etching together with the DLTS results reported by Fang *et al* [62], indicated that ICP etching caused monolayer-level interface roughness, disorder of the chemical bonds and formation of various types of defect complexes at the AlGaN surface, leading to poor *C–V* characteristics due to high-density interface states at the $Al_2O_3$/AlGaN interface. Tang *et al* [189] investigated $SiO_2$/*n*-GaN-based capacitors and FETs fabricated on etched GaN surfaces by $Cl_2$-based ICP. They demonstrated that ICP etching increased the interface state density and decreased the field-effect mobility in the FET channel. Kim *et al* [136] also reported that the ICP etching caused slight disorder of the chemical bonds at the GaN surface and monolayer-level interface roughness at the $Al_2O_3$/GaN interface, resulting in poor *C–V* characteristics due to high-density interface states including $V_N$-related levels.

### 4.3. Relevant characterization methods for HEMT MIS interfaces

The conductance method is often employed in HEMT MIS structures for analyzing interface states. Using this technique, careful attention should be given to the $E_F$ position at the insulator/AlGaN interface. For example, some papers reported conductance analysis in the reverse bias range on HEMT MIS structures [190–192]. At the reverse bias regime, however, the interface states could not be responsible for the conductance peak in the conductance–frequency (*G–f*) curve, because of their associated long emission time constants. Indeed, Shih *et al* [193] pointed out that the conventional conductance method is viable only for a narrow range of forward bias voltages, and invalid for the analysis of deeper interface states. In addition, Ramanan *et al* [194] and Yang *et al* [195] pointed out that the conductance method severely underestimates state densities at insulators/AlGaN (or InAlN) interfaces when a very thin AlN interlayer is included in the heterostructures. Shih *et al* [193] proposed a unique characterization method using forward-bias *G–f* characteristics at high temperatures. From an analysis based on the *G–f–T* (temperature) mapping, they estimated an energy range of interface states responding to the *G–f* measurement and gate-control efficiency related to an interface state density.

Frequency dispersion is one of characteristic features of an MIS gate on AlGaN/GaN heterostructures [104, 119, 196]. Fagerlind *et al* [197] and Hori *et al* [104] utilized the frequency dispersion characteristics of the *C–V* curves in the positive bias range for estimating interface state densities. They evaluated the MIS interface electronic state densities near the conduction-band edge for HEMT MIS structures. Recently, Yang *et al* [195] measured temperature- and frequency-dependent *C–V* characteristics of $Al_2O_3$/GaN/AlGaN/GaN structures in the temperature range from 25 to 200 °C and in the frequency range from 1 KHz to 10 MHz. They carried out a precise analysis on interaction between interface state and conduction band at each measurement temperature using the SRH statistics, and estimated $D_{it}(E)$ distribution at energies from

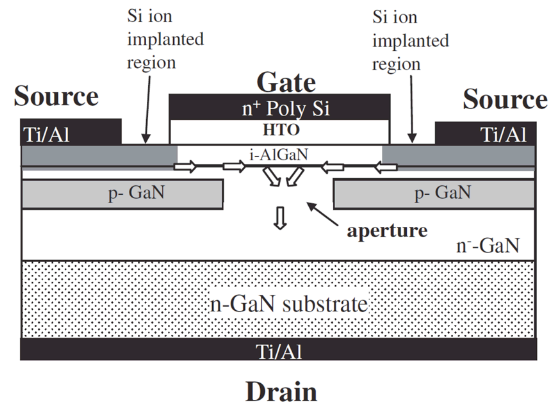


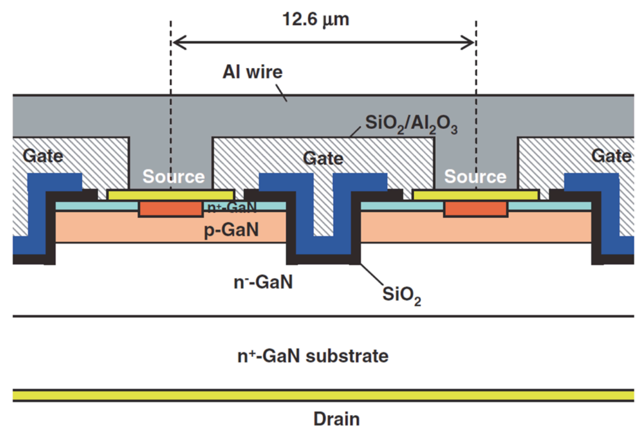


**Figure 17.** (a) Schematic illustration of the vertical GaN transistor with a combination of MOS HEMT channel and p-GaN blocking layer. (Reprinted with permission from [201], copyright 2007 by the Japan Society of Applied Physics.) (b) Trench-type n-channel GaN MOSFET. (Reprinted with permission from [205], copyright 2015 by the Japan Society of Applied Physics.)

$E_C - 0.2\,eV$ to $E_C - 0.8\,eV$. Yang *et al* [195] and Ramanan *et al* [194] applied a pulsed *I–V* method to $Al_2O_3$-gate AlGaN/GaN HEMTs and HfAlO-gate AlGaN/GaN HEMTs. From the $V_{TH}$ shift induced by either changing the pulse height or the quiescent gate voltage, they were also able to estimate the $D_{it}(E)$ distribution in their devices.

## 5. Recent progress in GaN MOS interfaces and MOS transistors

Significant progress in crystal growth of GaN and its related semiconductors enables us to obtain a free-standing GaN substrate and a homo-epitaxial GaN layer on GaN substrate with a relatively low dislocation density ($N_{DIS}$) of $1 \times 10^6$ cm$^{-2}$ or less. Kyle *et al* [198] reported a homo-epitaxial *n*-GaN ($N_{DIS} = 2 \times 10^6$ cm$^{-2}$) with a carrier density of $3.7 \times 10^{16}$ cm$^{-3}$ showing a mobility of 1265 cm$^2$ V$^{-1}$ s$^{-1}$ at RT and

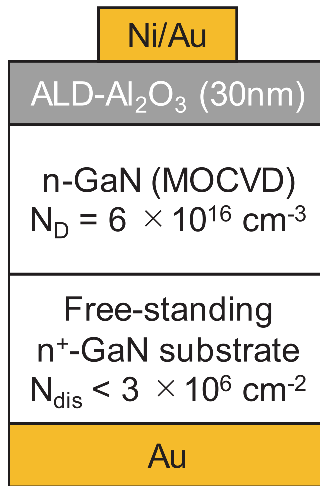


**Figure 18.** Schematic illustration of $Al_2O_3$/*n*-GaN/$n^+$-GaN structure.

3320 $cm^2$ $V^{-1}$ $s^{-1}$ at 113 K. Kizilyalli *et al* [199] fabricated $p^+n$ junction on a GaN substrate with $N_{DIS} = 1 \times 10^4$ $cm^{-2}$. The net doping density, $N_D$–$N_A$, and the thickness of the n-type drift layer were 2.0–5.0 × $10^{15}$ $cm^{-3}$ and 40 $\mu$m, respectively. They obtained a high breakdown voltage over 4 kV and low leakage currents at reverse bias up to the breakdown voltage. Hu *et al* [200] also reported excellent properties of GaN $p^+n$ diodes grown on a GaN substrate with a dislocation density of ~$10^6$ $cm^{-2}$. The $p^+n$ diode with an 8 $\mu$m drift layer ($N_D$–$N_A$ = 2.5 × $10^{15}$ $cm^{-3}$) showed a blocking voltage of over 1.4 kV and an $R_{ON}$ of 0.12 mΩ $cm^2$, giving the highest figure-of-merit ever reported in any semiconductor system. In addition, as described in the section 2.2, Schottky diodes on the GaN layers with a low dislocation density shows ideal *I*–*V* characteristics according to the simple TFE model. These results indicate highly improved crystalline quality of the current *n*-GaN epitaxial layers grown on GaN substrate.

The improved crystalline quality of GaN on GaN also has become a driving force for developing vertical-type GaN MIS transistors. Kanechika *et al* [201] reported a vertical GaN transistor with a combination of an MOS HEMT channel and a p-GaN blocking layer, as shown in figure 17(a). In this device, they used a selective regrowth of AlGaN/GaN layer and an $SiO_2$ gate structure. Chowdhury and co-workers [202, 203] reported a similar device using a Mg-implanted blocking layer and a SiN gate structure. Kodama *et al* [204] successfully fabricated a trench-type GaN MOSFET. For the trench structure, they used a combination of ICP dry etching and subsequent wet etching with tetramethylammonium hydroxide (TMAH). Recently, Oka *et al* [205] also reported a trench-type GaN MOSFET (figure 17(b)), demonstrating a blocking voltage over 1.2 kV, $V_{TH}$ of 3.5 V and $R_{ON}$ of 1.8 mΩ $cm^2$. It was expected that an ALD-deposited $SiO_2$ gate on the dry-etched p-GaN surface could realize device operation with an inverted channel. However, the $V_{TH}$ was much lower than the expected value calculated using the Mg doping density and the gate capacitance. The development of processing technologies such as ion implantation and healing

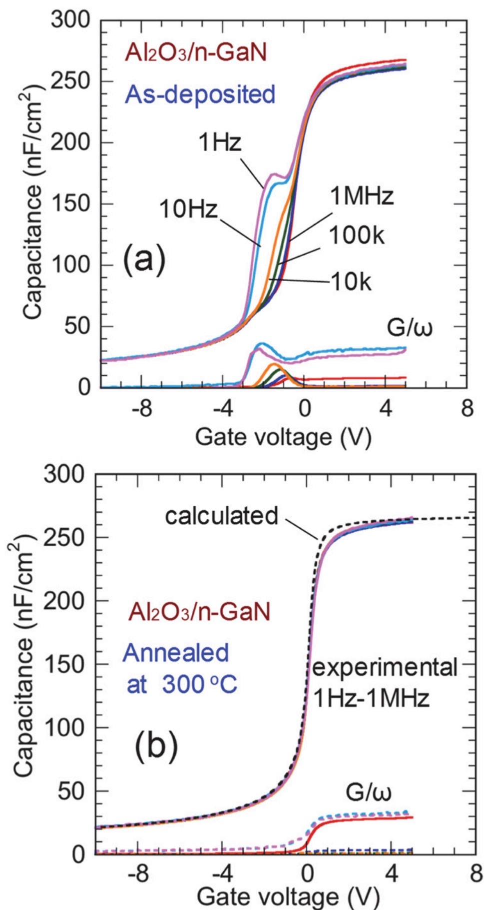


**Figure 19.** *C*–*V* characteristics of $Al_2O_3$/*n*-GaN/$n^+$-GaN MOS diodes (a) without and (b) with post-deposition annealing process obtained in wide measurement frequency range from 1 Hz to 1 MHz at RT.

of surface damage will improve the device performance of trench-type GaN MOSFETs.

A key issue for vertical type GaN MISFETs is still control of MIS interfaces. In this regard, we here introduce a stable GaN MOS interface with low densities of electronic states. Figure 18 shows the $Al_2O_3$/*n*-GaN MOS structure fabricated on a free-standing GaN substrate that we have recently investigated. An MOCVD *n*-GaN grown on an $n^+$-GaN substrate with relatively low dislocation density (<3 × $10^6$ $cm^{-2}$) was used. The $Al_2O_3$ layer with a nominal thickness of 30 nm was deposited on the GaN surface using an ALD system (SUGA-SAL1500) at 350 °C. In the deposition process, water vapor and TMA were introduced into a reactor in alternate pulse forms. Figure 19(a) shows RT *C*–*V* characteristics of the as-deposited MOS diode (without annealing) in a wide measurement frequency range of 1 Hz–1 MHz. The sample showed significant frequency dispersion at reverse bias. By lowering the frequency of the ac measurement signal, deeper interface states are expected to respond accordingly to an ac signal. This allows more of the states to follow the ac frequency and thereby contribute an additional component to the measured capacitance. On the other hand, excellent *C*–*V* characteristics with negligible frequency dispersion were observed in the MOS sample after annealing in air at 300 °C for 3 h under a

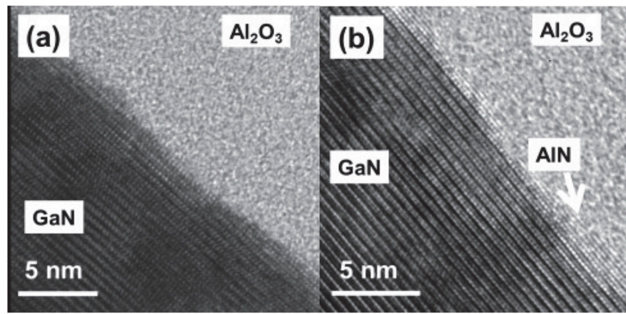


**Figure 20.** Cross-sectional TEM images of (a) $Al_2O_3$/GaN and (b) $Al_2O_3$/AlN/GaN interfaces. (Reprinted with permission from [154], copyright 2014 IEEE.)

reverse bias voltage of $-10$V, as shown in figure 19(b). The *C–V* curves of the bias-annealed sample are very close to the calculated curve (broken line) in a very wide frequency range of 1 Hz–1 MHz. In addition, there was no hysteresis in the *C–V* curve at RT with back and forth sweeping of gate voltage between $-10$ and 10V. Moreover, the *C–V* characteristics at 200 °C remained almost unchanged, as compared to the *C–V* curves at RT.

Although the reason for the improved *C–V* behavior after the reverse-bias annealing is not clarified yet, we think that relaxation of dangling bonds and defects at the GaN surface is enhanced under reverse bias condition. In III–V semiconductors with ionic bonding nature, deep levels or gap states often have strong interaction with the host lattice, e.g. EL2 level in GaAs and DX center in AlGaAs [206, 207], because of their localized wave functions. In this case, an electron occupation state (capture or emission of electron) at a deep level can be coupled with neighboring lattice vibration, causing lattice relaxation or distortion. During the reverse-bias annealing at 300 °C, it is expected that interface states and surface defect levels are empty of electrons. This can change bonding configuration of neighboring atoms, thereby leading to enhanced relaxation of dangling bonds and defects at the $Al_2O_3$/GaN interface. In case of the annealing at 300 °C under forward bias condition ($V_G = +5$V), we confirmed that the interface state density distribution was almost the same with that of the sample with the post-deposition annealing. Thus the electron occupation condition of interface states during the annealing process is an important factor for controlling interface state densities. Further study is necessary to understand the passivation mechanism on interface states.

These results indicate that the present process realizes a stable MOS interface with low interface state density less than $1 \times 10^{11}$ cm$^{-2}$ eV$^{-1}$ at around $E_C - 0.5$eV, when the MOS structure is fabricated on a high-quality GaN layer with a low dislocation density. However, during fabrication of a practical MOSFET, the GaN surface is usually subjected to dry-etching, ion-implantation and a high-temperature annealing processes. As mentioned in the previous section, these fabrication steps degrade MOS interface properties, i.e. increasing interface state densities or generating surface defects on the GaN surface. The next (final) step is the interface control of an insulated gate on the processed GaN surface.

As for HEMT devices, some control processes have been applied to insulated gate structures. Several groups [184, 208, 209] reported relatively good *C–V* characteristics and FET performances of MIS (MOS)-HEMTs using insulator-GaN/AlGaN/GaN structures (with a thin GaN cap layer), which are compatible to those of insulator-AlGaN/GaN structures. Recently, Ťapajna *et al* [196] reported almost same $D_{it}$ distribution for $Al_2O_3$-HEMT structures with and without a GaN cap layer. Van Hove *et al* [105] and Ronchi *et al* [210] demonstrated AlGaN/GaN HEMTs with stable threshold voltage ($V_{TH}$) and weak current collapse achieved using an *in situ* $SiN_x$/ALD-$Al_2O_3$ and an *in situ* $SiN_x$/PEALD- $SiN_x$ bilayer gates. Chan *et al* [211] reported that (Al, Si)O dielectric grown by MOCVD was attractive for achieving GaN MOS structures with low interface state densities. Liu *et al* [154] and Yang *et al* [212] applied a monolayer AlN as an interfacial layer to AlGaN/GaN MOS HEMTs with an ALD-$Al_2O_3$ gate, as shown in figure 20. They demonstrated small frequency dispersion in *C–V* characteristics of $Al_2O_3$/AlN/AlGaN/GaN MOS diodes and a small $V_{TH}$ shift in AlGaN/GaN MOS HEMTs. Application of insulated gates to InAlN/GaN HEMTs also leads to significant reduction of gate leakage currents and improvement of cutoff and maximum oscillation frequencies [213–215]. To control the $V_{TH}$ fluctuation in a normally-off HEMT, Nakazawa *et al* [216] demonstrated an $Al_2O_3$-gate AlGaN/GaN HEMT fabricated without using dry etching process. They carried out a selective regrowth of AlGaN on 5 nm AlGaN/GaN epi-layer in the source/drain and related access regions, and reported less $V_{TH}$ shift compared with the conventional recess-gate MOS HEMT fabricated by ICP dry etching.

Recently, Guo and del Alamo [217] carried out positive-bias temperature instability (PBTI) measurements on normally-off AlGaN/GaN MIS HEMTs using $SiO_2$ and $Al_2O_3$/$SiO_2$ as dielectric films, e.g. precise evaluation of changes in $V_{TH}$, SS and gate leakage current after applying positive bias stress to MIS HEMTs. They demonstrated that characteristics of the $V_{TH}$ shift and the SS increase induced by the positive bias stress are similar to those observed in Si, SiC and conventional III–V MOSFETs. Consequently, they proposed that such instability issues arise from two mechanisms: electron trapping in the oxide and generation of interface states at the oxide/GaN interface. Meanwhile, Meneghesso *et al* [218] reported significant correlation between the $V_{TH}$ shift and the leakage current under the positive bias stress of AlGaN/GaN MIS HEMTs with $SiN_x$ and $Al_2O_3$ dielectrics, pointing out that a possible reason for the $V_{TH}$ shift is electron trapping in the dielectric. Wu *et al* [219] also measured PBTI characteristics in recessed/insulated gate AlGaN/GaN MIS HEMTs with plasma-ALD $SiN_x$ and ALD $Al_2O_3$. They reported that gate dielectric defects inside the SiN are much more easily accessible under lower positive bias stress compared with $Al_2O_3$ gate dielectric, indicating that $Al_2O_3$ gate dielectric is indeed promising for improving the PBTI reliability. From the time-dependent dielectric breakdown (TDDB) measurement, Takashima *et al* [131] reported that the reliability of ALD-$SiO_2$/GaN structures were related to the surface treatment process of GaN before the $SiO_2$ deposition. Kachi [4] pointed out

that the TDDB lifetime of ALD $Al_2O_3$ at the electric field of 3 MV $cm^{-1}$ is more than 20 years, and hence it is applicable to power devices for automotive applications. Meneghesso *et al* [218] also measured the TDDB characteristics of AlGaN/GaN MIS HEMTs with $SiN_x$ and $Al_2O_3$ dielectrics. Since time to failure of devices indicated a Weibull distribution with slopes larger than 1.0, they demonstrated high robustness for ALD $SiN_x$ and $Al_2O_3$. For practical applications, stability and reliability characterization of GaN-based MIS transistors is becoming more and more relevant and important.

## 6. Summary

Although recent years have witnessed GaN-based devices delivering their promise of unprecedented performance and demonstrating their capability as an able replacement for Si-based devices, a practical and reliable approach towards associated stability and reliability issues should be developed. For widespread implementation and commercialization of GaN-based transistors, it is becoming undeniable that the MIS structure will play a major role.

For practical transistor applications, low leakage current, dependable current control, stable threshold voltage, high $g_m$ and wide dynamic range of input voltage are required from an MIS system. In view of these points, various GaN MIS structures were reviewed and discussed, particularly focusing on interface states that are deeply related to stability issues of MIS transistors. As for insulated gate applications, $SiO_2$ and $Al_2O_3$ are considered attractive insulator materials due to their favorable dielectric properties such as large bandgap and high chemical stability. With suitable pre-deposition treatment and post-deposition annealing, stable $SiO_2$/GaN and $Al_2O_3$/GaN structures with low interface state densities using epitaxial GaN crystals can be achieved as reported in literature. The remaining issue is the interface control of the MOS structures fabricated on the processed GaN surfaces such as those subjected to dry-etching, ion-implantation and high-temperature annealing steps. Although the bandgap of $SiN_x$ (~5.0 eV) is not sufficiently large for the insulated gate application, $SiN_x$ is an important material for surface passivation of GaN-based transistors. In particular, *in situ* deposition of $SiN_x$ during the MOCVD growth process can improve the operation stability of GaN HEMTs. Various types of high-$\kappa$ insulators have also been applied to the gate structures of GaN transistors. However, further investigation on chemical stability and interface properties of high-$\kappa$/GaN structures is still needed.

For a MIS gate structure application to AlGaN/GaN or InAlN/GaN heterostructures, characterization of electronic state properties at the insulator/AlGaN (InAlN) interfaces critical to device operation is very important. On this account, we reviewed pertinent results from literature including accurate *C*–*V* calculation, photo-assisted *C*–*V*, conductance, frequency- and temperature-dependent conductance, frequency-dependent *C*–*V* and pulsed *I*–*V* methods. Using the combination of numerical fitting of *C*–*V* curves and photo-assisted *C*–*V* method, the state density distributions of the $Al_2O_3$/AlGaN interfaces were determined in the energy range between $E_C$ and midgap.

In summary, in this work, we have described critical issues and problems including leakage current, current collapse and threshold voltage instability in GaN-based HEMTs. The nature and characteristics of different AlGaN/GaN MIS structures essential for achieving successful surface passivation and interface control schemes were also discussed. Lastly, we highlighted important current progress in GaN MIS interfaces that have recently pushed the frontier of nitride-based device technology. On the final note, nevertheless, we believe that further investigation and understanding of interface states are absolutely necessary for achieving reliable and unquestionable operation stability in GaN-based MIS transistors including MIS HEMTs.

## Acknowledgments

On of the authors (TH) would like to thank the support by Council for Science, Technology and Innovation (CSTI), Cross-ministerial Strategic Innovation Promotion Program (SIP), 'Next-generation power electronics' (funding agency: NEDO).

## References

[1] Lee D S, Liu Z and Palacios T 2014 *Japan. J. Appl. Phys.* **53** 100212
[2] Shinohara K *et al* 2013 *IEEE Trans. Electron Devices* **60** 2982
[3] Ueda T, Ishida M, Tanaka T and Ueda D 2014 *Japan. J. Appl. Phys.* **53** 100214
[4] Kachi T 2014 *Japan. J. Appl. Phys.* **53** 100210
[5] Dora Y, Chakraborthy A, McCarthy L, Keller S, DenBaars S P and Mishra U K 2006 *IEEE Electron Device Lett.* **27** 713
[6] Choi Y C, Pophristic M, Peres B, Spencer M G and Eastman L F 2006 *J. Vac. Sci. Technol.* B **24** 2601
[7] Tipirneni N, Koudymov A, Adivarahan V, Yang J, Simin G and Khan M A 2006 *IEEE Electron Device Lett.* **27** 716
[8] Bahat-Treidel E, Brunner F, Hilt O, Cho E, Wurfl J and Trankle G 2010 *IEEE Trans. Electron Devices* **57** 3050
[9] Lee J-G, Park B-R, Lee H-J, Lee M, Seo K-S and Cha H-Y 2012 *Appl. Phys. Express* **5** 066502
[10] Lee H S, Piedra D, Sun M, Gao X, Guo S and Palacios T 2012 *IEEE Electron Device Lett.* **33** 982
[11] Christy D, Egawa T, Yano Y, Tokunaga H, Shimamura H, Yamaoka Y, Ubukata A, Tabuchi T and Matsumoto K 2013 *Appl. Phys. Express* **6** 026501
[12] Seok O, Ahn W, Han M-K and Ha M-W 2013 *Electron. Lett.* **49** 425
[13] Herbecq N, Roch-Jeune I, Rolland N, Visalli D, Derluyn J, Degroote S, Germain M and Medjdoub F 2014 *Appl. Phys. Express* **7** 034103
[14] Kuzuhara M and Tokuda H 2015 *IEEE Trans. Electron Devices* **62** 405
[15] Herbecq N, Roch-Jeune I, Linge A, Grimbert B, Zegaoui M and Medjdoub F 2015 *Electron. Lett.* **51** 1532
[16] Yanagihara M, Uemoto Y, Ueda T, Tanaka T, Ueda D 2009 *Phys. Status Solidi* a **206** 1221
[17] Chung J W, Kim T-W and Palacios T 2010 *Int. Electron Decvices Meeting Tech Digest* 30.2.1
[18] Lee D S, Laboutin O, Cao Y, Johnson W, Beam E, Ketterson A, Schuette M, Saunier P and Palacios T 2012 *IEEE Electron Device Lett.* **33** 976

[19] Tang Y, Shinohara K, Regan D, Corrion A, Brown D, Wong J, Schmitz A, Fung H, Kim S and Micovic M 2015 *IEEE Electron Device Lett.* **36** 549

[20] Green B M, Chu K K, Chumbes E M, Smart J A, Shealy J R and Eastman L F 2000 *IEEE Electron Device Lett.* **21** 268

[21] Hashizume T, Ootomo S, Inagaki T and Hasegawa H 2003 *J. Vac. Sci. Technol.* B **21** 1828

[22] del Alamo J A 2011 *Nature* **479** 317

[23] Yokoyama M *et al* 2011 *IEEE Electron Device Lett.* **32** 1218

[24] Takagi S *et al* 2013 *Solid-State Electron.* **88** 2

[25] Ye P D *et al* 2003 *IEEE Electron Device Lett.* **24** 209

[26] Ye P D, Xuan Y, Wu Y Q and Xu M 2009 *ECS Trans.* **19** 605

[27] Bentley S J *et al* 2011 *IEEE Electron Device Lett.* **32** 494

[28] Li Q, Zhou X, Tang C W and Lau K M 2012 *IEEE Electron Device Lett.* **33** 1246

[29] Jiao G, Yao C, Xuan Y, Huang D, Ye P D and Li M-F 2012 *IEEE Trans. Electron Devices* **59** 1661

[30] Hasegawa H and Sawada T 1980 *IEEE Trans. Electron Devices* **27** 1055

[31] Hinkle C L, Sonnet A M, Milojevic M, Aguirre-Tostado F S, Kim H C, Kim J, Wallace R M and Vogel E M 2008 *Appl. Phys. Lett.* **93** 1113506

[32] Galatage R V, Dong H, Zhernokletov D M, Brennan B, Hinkle C L, Wallace R M and Vogel E M 2011 *Appl. Phys. Lett.* **99** 172901

[33] Xuan Y, Wu Y Q, Lin H C, Shen T and Ye P D 2007 *IEEE Electron Device Lett.* **28** 935

[34] Goel N, Majhi P, Tsai W, Warusawithana M, Schlom D G, Santos M B, Harris J S and Nishi Y 2007 *Appl. Phys. Lett.* **91** 093509

[35] Koveshnikov S *et al* 2008 *Appl. Phys. Lett.* **92** 222904

[36] Galatage R V, Zhernokletov D M, Dong H, Brennan B, Hinkle C L, Wallace R M and Vogel E M 2014 *J. Appl. Phys.* **116** 014504

[37] Yuan Y, Wang L, Yu B, Shin B, Ahn J, McIntyre P C, Asbeck P M, Rodwell M J W and Taur Y 2011 *IEEE Electron Device Lett.* **32** 485

[38] Chen H-P, Yuan Y, Yu B, Ahn J, McIntyre P C, Asbeck P M, Rodwell M J W and Taur Y 2012 *IEEE Trans. Electron Devices* **59** 2383

[39] Brammertz G, Alian A, Lin D H-C, Meuris M, Caymax M and Wang W-E 2011 *IEEE Trans. Electron Devices* **58** 3890

[40] Hasegawa H and Ohno H 1986 *J. Vac. Sci. Technol.* B **4** 1130

[41] He L, Hasegawa H, Sawada T and Ohno H 1988 *J. Appl. Phys.* **63** 2120

[42] Mizue C, Hori Y, Miczek M and Hashizume T 2011 *Japan. J. Appl. Phys.* **50** 021001

[43] Eller B S, Yang J and Nemanich R J 2013 *J. Vac. Sci. Technol.* A **31** 050807

[44] Roccaforte F, Fiorenza P, Greco G, Vivona M, Lo Nigro R, Giannazzo F, Patti A and Saggio M 2014 *Appl. Surf. Sci.* **301** 9

[45] del Alamo J A and Joh J 2009 *Microelectron. Reliab.* **49** 1200

[46] Wu Y, Chen C-Y and del Alamo J A 2015 *J. Appl. Phys.* **117** 025707

[47] Marko P, Meneghini M, Bychikhin S, Marcon D, Meneghesso G, Zanoni E and Pogany D 2012 *Microelectron. Reliab.* **52** 12194

[48] Cullen D A, Smith D J, Passaseo A, Tasco V, Stocco A, Meneghini M, Meneghesso G and Zanoni E 2013 *IEEE Trans. Devices Mater. Relaib.* **13** 126

[49] Zanoni E, Meneghini M, Chini A, Marcon D and Meneghesso G 2013 *IEEE Trans. Electron Devices* **60** 3119

[50] Yu L S, Liu Q Z, Xing Q J, Qiao D J, Lau S S and Redwing J 1998 *J. Appl. Phys.* **84** 2099

[51] Miller E J, Dang X Z and Yu E T 2000 *J. Appl. Phys.* **88** 5951

[52] Miller E J, Yu E T, Waltereit P and Speck J S 2004 *Appl. Phys. Lett.* **84** 535

[53] Carrano J C, Li T, Grudowski P A, Eiting C J, Dupuis R D and Cambell J C 1998 *Appl. Phys. Lett.* **72** 542

[54] Karmalkar S, Sathaiya D M and Shur M S 2003 *Appl. Phys. Lett.* **82** 3976

[55] Sawada T, Ito Y, Imai K, Suzuki K, Tomozawa H and Sakai S 2000 *Appl. Surf. Sci.* **159–60** 449

[56] Kotani J, Hashizume T and Hasegawa H 2004 *J. Vac. Sci. Technol.* B **22** 2179

[57] Hashizume T, Kotani J and Hasegawa H 2004 *Appl. Phys. Lett.* **84** 4884

[58] Hashizume T and Nakasaki R 2002 *Appl. Phys. Lett.* **80** 4564

[59] Hashizume T and Hasegawa H 2004 *Appl. Surf. Sci.* **234** 387

[60] Kuzmík J, Javorka P, Marso M and Kordos P 2002 *Semicond. Sci. Technol.* **17** L76

[61] Lee C Y, Sekiguchi H, Okada H and Wakahara A 2012 *Japan. J. Appl. Phys.* **51** 076503

[62] Fang Z-Q, Look D C, Wang X-L, Han J, Khan F A and Adesida I 2003 *Appl. Phys. Lett.* **82** 1562

[63] Yatabe Z, Hori Y, Kim S and Hashizume T 2013 *Appl. Phys. Express* **6** 016502

[64] Hayashi K, Yamaguchi Y, Oishi T, Otsuka H, Yamanaka K, Nakayama M and Miyamoto Y 2013 *Japan. J. Appl. Phys.* **52** 04CF12

[65] Suda J, Yamaji K, Hayashi Y, Kimoto T, Shimoyama K, Namita H and Nagao S 2010 *Appl. Phys. Express* **3** 101003

[66] Lugani L, Py M A, Carlin J-F and Grandjean N 2014 *J. Appl. Phys.* **115** 074506

[67] Kotani J, Yamada A, Ishiguro T, Tomabechi S and Nakamura N 2016 *Appl. Phys. Lett.* **108** 152109

[68] Khan M A, Shur M S, Chen Q C and Kuznia J N 1994 *Electron. Lett.* **30** 2175

[69] Vetury R, Zhang N Q, Keller S and Mishra U K 2001 *IEEE Trans. Electron Devices* **48** 560

[70] Trew R J, Green D S and Shealy J B 2009 *IEEE Microw. Mag.* **10** 116

[71] Saito W, Nitta T, Kakiuchi Y, Saito Y, Tsuda K, Omura I and Yamaguchi M 2007 *IEEE Trans. Electron Devices* **54** 1825

[72] Arulkumaran S, Ng G I, Lee C H, Liu Z H, Radhakrishnan K, Dharmarasu N and Sun Z 2010 *Solid-State Electron.* **54** 1430

[73] Kotani J, Tajima M, Kasai S and Hashizume T 2007 *Appl. Phys. Lett.* **91** 093501

[74] Cardwell D W, Arehart A R, Poblenz C, Pei Y, Speck J S, Mishra U K, Ringel S A and Pelz J P 2012 *Appl. Phys. Lett.* **100** 193507

[75] Katsuno T, Manaka T, Ishikawa T, Ueda H, Uesugi T and Iwamoto M 2014 *Appl. Phys. Lett.* **104** 252112

[76] Tajima M and Hashizume T 2011 *Japan. J. Appl. Phys.* **50** 061001

[77] Nishiguchi K, Asubar J T and Hashizume T 2014 *Japan. J. Appl. Phys.* **53** 070301

[78] Nakajima A, Fujii K and Horio K 2011 *Japan. J. Appl. Phys.* **50** 104303

[79] Faramehr S, Kalna K and Igić P 2014 *Semicond. Sci. Technol.* **29** 025007

[80] Chen S, Honda U, Shibata T, Matsumura T, Tokuda Y, Ishikawa K, Hori M, Ueda H, Uesugi T and Kachi T 2012 *J. Appl. Phys.* **112** 053513

[81] Duc T T, Pozina G, Janzén E and Hemmingsson C 2013 *J. Appl. Phys.* **114** 153702

[82] Karmalkar S and Mishra U K 2001 *IEEE Trans. Electron Devices* **48** 1515

[83] Ando Y, Okamoto Y, Miyamoto H, Nakayama T, Inoue T and Kuzuhara M 2003 *IEEE Electron Device Lett.* **24** 289

[84] Okamoto Y *et al* 2004 *IEEE Trans. Electron Devices* **51** 2217

[85] Saito W, Nitta T, Kakiuchi Y, Saito Y, Tsuda K, Omura I and Yamaguchi M 2007 *IEEE Electron Device Lett.* **28** 676

[86] Hasan M T, Asano T, Tokuda H and Kuzuhara M 2013 *IEEE Trans. Electron Devices* **34** 1379

[87] Ohi K, Asubar J T, Nishiguchi K and Hashizume T 2013 *IEEE Trans. Electron Devices* **60** 2997
[88] Asubar J, Ohi K, Nishiguchi K and Hashizume T 2014 *Phys. Status Solidi* c **11** 857
[89] Nakasaki R, Hashizume T and Hasegawa H 2000 *Physica* E **7** 953
[90] Kim H, Thompson R M, Tilak V, Prunty T R, Shealy J R and Eastman L F 2003 *IEEE Electron Device Lett.* **24** 421
[91] Bae C, Krug C, Lucovsky G, Chakraborty A and Mishra U 2004 *J. Appl. Phys.* **96** 2674
[92] Derluyn J, Boeykens S, Cheng K, Vandersmissen R, Das J, Ruythooren W, Degroote S, Leys M R, Germain M and Borghs G 2005 *J. Appl. Phys.* **98** 054501
[93] Coffie R, Buttari D, Heikman S, Keller S, Chini A, Shen L and Mishra U K 2002 *IEEE Electron Device Lett.* **23** 588
[94] Shen L, Coffie R, Buttari D, Heikman S, Chakraborty A, Chini A, Keller S, DenBaars S P and Mishra U K 2004 *IEEE Trans. Electron Devices* **25** 7
[95] Kikkawa T 2005 *Japan. J. Appl. Phys.* **44** 4896
[96] Lu Y, Yang S, Jiang Q, Tang Z, Li B and Chen K J 2013 *Phys. Status Solidi* c **10** 1397
[97] Ťapajna M, Jurkovič M, Válik L, Haščík Š, Gregušová D, Brunner F, Cho E-M and Kuzmík J 2013 *Appl. Phys. Lett.* **102** 243509
[98] Johnson D W, Lee R T P, Hill R J W, Wong M H, Bersuker G, Piner E L, Kirsch P D and Harris H R 2013 *IEEE Trans. Electron Devices* **60** 3197
[99] Lagger P *et al* 2014 *Appl. Phys. Lett.* **105** 033512
[100] Wu T-L *et al* 2015 *Appl. Phys. Lett.* **107** 093507
[101] Esposto M, Krishnamoorthy S, Nath D N, Bajaj S, Hung T-H and Rajan S 2011 *Appl. Phys. Lett.* **99** 133503
[102] Son J, Chobpattana V, McSkimming B M and Stemmer S 2012 *Appl. Phys. Lett.* **101** 102905
[103] Yang S, Tang Z, Wong K-Y, Lin Y-S, Liu C, Lu Y, Huang S and Chen K J 2013 *IEEE Electron Device Lett.* **34** 1497
[104] Hori Y, Yatabe Z and Hashizume T 2013 *J. Appl. Phys.* **114** 244503
[105] Van Hove M, Kang X, Stoffels S, Wellekens D, Ronchi N, Venegas R, Geens K and Decoutere S 2013 *IEEE Trans. Electron Devices* **60** 3071
[106] Robertson J and Falabretti B 2006 *J. Appl. Phys.* **100** 014111
[107] Mönch W 1997 *Appl. Surf. Sci.* **117/118** 380
[108] Gaffey B, Guido L J, Wang X W and Ma T P 2001 *IEEE Trans. Electron Devices* **48** 458
[109] Cook T E Jr, Fulton C C, Mecouch W J, Tracy K M, Davis R F, Hurt E H, Lucovsky G and Nemanich R J 2003 *J. Appl. Phys.* **93** 3995
[110] Yang J, Eller B S and Nemanich R J 2014 *J. Appl. Phys.* **116** 123702
[111] Cook T E Jr, Fulton C C, Mecouch W J, Davis R F, Lucovsky G and Nemanich R J 2003 *J. Appl. Phys.* **94** 3949
[112] Hamsen C, Lorenz P, Schaefer J A and Krischok S 2010 *Phys. Status Solidi* c **7** 268
[113] Lee C-T, Lee H-Y and Chen H-W 2003 *IEEE Electron Device Lett.* **24** 54
[114] Lay T S, Liao Y Y, Hung W H, Hong M, Kwo J and Mannaerts J P 2005 *J. Cryst. Growth* **278** 624
[115] Cook T E Jr, Fulton C C, Mecouch W J, Davis R F, Lucovsky G and Nemanich R J 2003 *J. Appl. Phys.* **94** 7155
[116] Tian F and Chor E F 2010 *Thin Solid Films* **518** e121
[117] Chang W H *et al* 2009 *Adv. Mater.* **21** 4970
[118] Ihlefeld J F, Brumbach M and Atcitty S 2013 *Appl. Phys. Lett.* **102** 162903
[119] Qin X, Cheng L, McDonnell S, Azcatl A, Zhu H, Kim J and Wallace R M 2015 *J. Mater. Sci., Mater. Electron.* **26** 4638
[120] Miyazaki S 2001 *J. Vac. Sci. Technol.* B **19** 2212
[121] Huang M L, Chang Y C, Chang Y H, Lin T D, Kwo J and Hong M 2009 *Appl. Phys. Lett.* **94** 052106
[122] Khan M A, Hu X, Sumin G, Lunev A, Yang J, Gaska R and Shur M S 2000 *IEEE Trans. Electron Devices* **21** 63
[123] Hu X, Koudymov A, Simin G, Yang J, Asif Khan M, Tarakji A, Shur M S and Gaska R 2001 *Appl. Phys. Lett.* **79** 2832
[124] Matocha K, Gutmann R J and Chow T P 2003 *IEEE Trans. Electron Devices* **50** 1200
[125] Kim E, Soejima N, Watanabe Y, Ishiko M and Kachi T 2010 *Japan. J. Appl. Phys.* **49** 04DF08
[126] Niiyama Y, Shinagawa T, Ootomo S, Kambayashi H, Nomura T and Yoshida S 2007 *Phys. Status Solidi* a **204** 2032
[127] Huang W, Khan T and Chow T P 2006 *IEEE Electron Devices Lett.* **27** 796
[128] Kambayashi H, Satoh Y, Ootomo S, Kokawa T, Nomura T, Kato S and Chow T P 2010 *Solid-State Electron.* **54** 660
[129] Yamaji K, Noborio M, Suda J and Kimoto T 2008 *Japan. J. Appl. Phys.* **47** 7784
[130] Kirkpatrick C J, Lee B, Suri R, Yang X and Misra V 2012 *IEEE Electron Device Lett.* **33** 1240
[131] Takashima S, Li Z and Chow T P 2013 *Japan. J. Appl. Phys.* **52** 08JN24
[132] Kambayashi H, Nomura T, Ueda H, Harada K, Morozumi Y, Hasebe K, Teramoto A, Sugawa S and Ohmi T 2013 *Japan. J. Appl. Phys.* **52** 04CF09
[133] Park K-Y, Cho H-I, Lee J-H, Bae S-B, Jeon C-M, Lee J-L, Kim D-Y, Lee C-S and Lee J-H 2003 *Phys. Status Solidi* c **0** 2351
[134] Ye P D, Yang B, Ng K K and Bude J, Wilk G D, Halder S and Hwang J C M 2005 *Appl. Phys. Lett.* **86** 063501
[135] Hori Y, Mizue C and Hashizume T 2010 *Japan. J. Appl. Phys.* **49** 080201
[136] Kim S, Hori Y, Ma W-C, Kikuta D, Narita T, Iguchi H, Uesugi T, Kachi T and Hashizume T 2012 *Japan. J. Appl. Phys.* **51** 060201
[137] Toyoda S, Shinohara T, Kumigashira H, Oshima M and Kato Y 2012 *Appl. Phys. Lett.* **101** 231607
[138] Choi M, Lyons J L, Janotti A and Van de Walle C G 2013 *Phys. Status Solidi* b **250** 787
[139] Kikuta D, Narita T, Kutsuki K, Uesugi T and Kachi T 2013 *Japan. J. Appl. Phys.* **52** 08JN19
[140] Medjdoub F, Van Hove M, Cheng K, Marcon D, Leys M and Decoutere S 2010 *IEEE Electron Device Lett.* **31** 948
[141] Greco G, Fiorenza P, Giannazzo F, Alberti A and Roccaforte F 2014 *Nanotechnology* **25** 025201
[142] Wolter S D, DeLucca J M, Mohney S E, Kern R S and Kuo C P 2000 *Thin Solid Films* **371** 153
[143] Zhou Y *et al* 2008 *Solid-State Electron.* **52** 756
[144] Roccaforte F, Giannazzo F, Iucolano F, Bongiorno C and Raineri V 2009 *J. Appl. Phys.* **106** 023703
[145] Mistele D *et al* 2002 *Mater. Sci. Eng.* B **93** 107
[146] Harada N, Hori Y, Azumaishi N, Ohi K and Hashizume T 2011 *Appl. Phys. Express* **4** 021002
[147] Romero M-F, Jiménez A, González-Posada Flores F, Martín-Horcajo S, Calle F and Muñoz E 2012 *IEEE Trans. Electron Devices* **59** 374
[148] Ochiai M, Akita M, Ohno Y, Kishimoto S, Maezawa K and Mizutani T 2003 *Japan. J. Appl. Phys.* **42** 2278
[149] Chini A, Wittich J, Heikman S, Keller S, DenBaars S P and Mishra U K 2004 *IEEE Electron Device Lett.* **25** 55
[150] Ogawa E, Hashizume T, Nakazawa S, Ueda T and Tanaka T 2007 *Japan. J. Appl. Phys.* **46** L590
[151] Takizawa T, Nakazawa S and Ueda T 2008 *J. Electron. Mater.* **37** 628
[152] Hashizume T, Alekseev E, Pavlidis D, Boutros K S and Redwing J 2000 *J. Appl. Phys.* **88** 1983
[153] Tsurumi N, Ueno H, Murata T, Ishida H, Uemoto Y, Ueda T, Inoue K and Tanaka T 2010 *IEEE Trans. Electron Devices* **57** 980

[154] Liu S, Yang S, Tang Z, Jiang Q, Liu C, Wang M and Chen K J 2014 *IEEE Electron Device Lett.* **35** 723
[155] Deen D, Storm D, Meyer D, Katzer D S, Bass R, Binari S and Gougousi T 2011 *Phys. Status Solidi* c **8** 2420
[156] Kikkawa T, Makiyama K, Ohki T, Kanamura M, Imanishi K, Hara N and Joshin K 2009 *Phys. Status Solidi* a **206** 1135
[157] Yang S, Huang S, Schnee M, Zhao Q-T, Schubert J and Chen K J 2013 *IEEE Trans. Electron Devices* **60** 3040
[158] Hatano M, Taniguchi Y, Kodama S, Tokuda H and Kuzuhara M 2014 *Appl. Phys. Express* **7** 044101
[159] Roccaforte F, Greco G, Fiorenza P, Raineri V, Malandrino G and Lo Nigro R 2012 *Appl. Phys. Lett.* **100** 063511
[160] Fiorenza P, Greco G, Giannazzo F, Lo Nigro R and Roccaforte F 2012 *Appl.Phys. Lett.* **101** 172901
[161] Fiorenza P, Greco G, Fisichella G, Roccaforte F, Malandrino G and Lo Nigro R 2013 *Appl. Phys. Lett.* **103** 112905
[162] Chiu Y S, Liao J T, Lin Y C, Liu S C, Lin T M, Iwai H, Kakushima K and Chang E Y 2016 *Japan. J. Appl. Phys.* **55** 051001
[163] Colón A and Shi J 2014 *Solid-State Electron.* **99** 25
[164] Hayashi Y, Kishimoto S and Mizutani T 2010 *Solid-State Electron.* **54** 1451
[165] Stoklas R, Gregušová D, Hušeková K, Marek J and Kordoš P 2014 *Semicond. Sci. Technol.* **29** 045003
[166] Hossain T, Wei D, Edgar J H, Garces N Y, Nepal N, Hite J K, Mastro M A, Eddy C R Jr and Meyer H M III 2015 *J. Vac. Sci. Technol.* B **33** 061201
[167] Chakroun A, Maher H, Al Alam E, Souifi A, Aimez V, Arès R and Jaouad A 2014 *IEEE Electron Device Lett.* **35** 318
[168] Chen K J, Yang S, Tang Z, Huang S, Lu Y, Jiang Q, Liu S, Liu C and Li B 2015 *Phys. Status Solidi* a **212** 1059
[169] Winzer A, Szabo N, Wachowiak A, Jordan P M, Heitmann J and Mikolajick T 2015 *J. Vac. Sci. Technol.* B **33** 01A106
[170] Long R D *et al* 2013 *Appl. Phys. Lett.* **103** 201607
[171] Yue Y, Hao Y, Zhang J, Ni J, Mao W, Feng Q and Liu L 2008 *IEEE Electron Device Lett.* **29** 838
[172] Tian F and Chor E F 2010 *J. Electrochem. Soc.* **157** H557
[173] Shi J and Eastman L F 2011 *IEEE Electron Device Lett.* **32** 312
[174] Miczek M, Mizue C, Hashizume T and Adamowicz B 2008 *J. Appl. Phys.* **103** 104510
[175] Yatabe Z, Hori Y, Ma W-C, Asubar J T, Akazawa M, Sato T and Hashizume T 2014 *Japan. J. Appl. Phys.* **53** 100213
[176] Lüth H 1993 *Surfaces and Interfaces of Solids* 2nd edn (Berlin: Springer) p 262 and 382
[177] Mönch W 2011 *J. Appl. Phys.* **109** 113724
[178] Shockley W and Read W T Jr 1952 *Phys. Rev.* **87** 835
[179] Tersoff J 1984 *Phys. Rev. Lett.* **52** 465
[180] Ye P D 2008 *J. Vac. Sci. Technol.* A **31** 697
[181] Osvald J, Stoklas R and Kordos P 2015 *Phys. Status Solidi* b **252** 996
[182] Liu Z H, Ng G I, Arulkumaran S, Maung Y K T, Teo K L, Foo S C and Sahmuganathan V 2009 *Appl. Phys. Lett.* **95** 223501
[183] Selvaraj S L and Egawa T 2009 *J. Electrochem. Soc.* **156** H690
[184] Ozaki S, Ohki T, Kanamura M, Okamoto N and Kikkawa T 2013 *Japan. J. Appl. Phys.* **52** 11NG04
[185] Yeluri R, Swenson B L and Mishra U K 2012 *J. Appl. Phys.* **111** 043718
[186] Fagerlind M and Rorsman N 2012 *J. Appl. Phys.* **112** 014511
[187] Matys M, Adamowicz B and Hashizume T 2012 *Appl. Phys. Lett.* **101** 231608
[188] Matys M, Adamowicz B, Hori Y and Hashizume T 2013 *Appl. Phys. Lett.* **103** 021603
[189] Tang K, Huang W and Chow T P 2009 *J. Electron. Mater.* **38** 523
[190] Freedsman J J, Kubo T and Egawa T 2011 *Appl. Phys. Lett.* **99** 033504
[191] Ye G, Wang H, Arulkumaran S, Ng G I, Hofstetter R, Li Y, Anand M J, Ang K S, Maung Y K T and Foo S C 2013 *Appl. Phys. Lett.* **103** 142109
[192] Pérez-Tomás A, Fontserè A, Sánchez S, Jennings M R, Gammon P M and Cordier Y 2013 *Appl. Phys. Lett.* **102** 023511
[193] Shih H-A, Kudo M and Suzuki T 2012 *Appl. Phys. Lett.* **101** 043501
[194] Ramanan N, Lee B and Misra V 2015 *IEEE Trans. Electron Devices* **62** 546
[195] Yang S, Liu S, Lu Y, Liu C and Chen K J 2015 *IEEE Trans. Electron Devices* **62** 1870
[196] Ťapajna M, Jurkovič M, Válik L, Haščík Š, Gregušová D, Brunner F, Cho E-M, Hashizume T and Kuzmík J 2014 *J. Appl. Phys.* **116** 104501
[197] Fagerlind M, Allerstam F, Sveinbjörnsson E Ö, Rorsman N, Kakanakova-Georgieva A, Lundskog A, Forsberg U and Janzén E 2010 *J. Appl. Phys.* **108** 014508
[198] Kyle E C H, Kaun S W, Burke P G, Wu F, Wu Y-R and Speck J S 2014 *J. Appl. Phys.* **115** 193702
[199] Kizilyalli I C, Prunty T and Aktas O 2015 *IEEE Electron Device Lett.* **36** 1073
[200] Hu Z, Nomoto K, Song B, Zhu M, Qi M, Pan M, Gao X, Protasenko V, Jena D and Xing H G 2015 *Appl. Phys. Lett.* **107** 243501
[201] Kanechika M, Sugimoto M, Soejima N, Ueda H, Ishiguro O, Kodama M, Hayashi E, Itoh K, Uesugi T and Kachi T 2007 *Japan. J. Appl. Phys.* **46** L503
[202] Chowdhury S, Wong M H, Swenson B L and Mishra U K 2012 *IEEE Electron Device Lett.* **33** 41
[203] Chowdhury S and Mishra U K 2013 *IEEE Trans. Electron Devices* **60** 3060
[204] Kodama M, Sugimoto M, Hayashi E, Soejima N, Ishiguro O, Kanechika M, Itoh K, Ueda H, Uesugi T and Kachi T 2008 *Appl. Phys. Express* **1** 021104
[205] Oka T, Ina T, Ueno Y and Nishii J 2015 *Appl. Phys. Express* **8** 054101
[206] Vincent G and Bois D 1978 *Solid State Commun.* **27** 431
[207] Lang D V, Rogan R A and Jaros M 1979 *Phys. Rev.* B **19** 1015
[208] Mehari S S, Yalon E, Gavrilov A, Mistele D, Bahir G, Eizenberg M and Ritter D 2014 *IEEE Trans. Electron Devices* **61** 3558
[209] Zhu J-J, Ma X-H, Xie Y, Hou B, Chen W-W, Zhang J-C and Hao Y 2015 *IEEE Trans. Electron Devices* **62** 512
[210] Ronchi N, De Jaeger B, Van Hove M, Roelofs R, Wu T-L, Hu J, Kang X and Decoutere S 2015 *Japan. J. Appl. Phys.* **54** 04DF02
[211] Chan S H *et al* 2016 *Japan. J. Appl. Phys.* **55** 021501
[212] Yang S, Liu S, Liu C, Hua M and Chen K J 2016 *Semicond. Sci. Technol.* **31** 024001
[213] Kuzmik J, Pozzovivo G, Abermann S, Carlin J-F, Gonschorek M, Feltin E, Grandjean N, Bertagnolli E, Strasser G and Pogany D 2008 *IEEE Trans. Electron Devices* **55** 937
[214] Yue Y *et al* 2012 *IEEE Electron Device Lett.* **33** 988
[215] Akazawa M 2014 *Japan. J. Appl. Phys.* **53** 028003
[216] Nakazawa S, Shiozaki N, Negoro N, Tsurumi N, Anda Y, Ishida M and Ueda T 2015 *Int. Conf. Solid State Devices and Materials (SSDM-2015) (Sapporo, Japan, 28–30 September 2015*) Abstract M-2–3
[217] Guo A and del Alamo J A 2015 *Proc. of the IEEE Int. Reliability Physics Symp. (IRPS)* p 6C.5.1
[218] Meneghesso G, Meneghini M, Bisi D, Rossetto I, Wu T-L, Van Hove M, Marcon D, Stoffels S, Decoutere S and Zanoni E 2016 *Microelectron. Reliab.* **58** 151
[219] Wu T-L, Franco J, Marcon D, De Jaeger B, Bakeroot B, Stoffels S, Van Hove M, Groeseneken G and Decoutere S 2016 *IEEE Trans. Electron Devices* **63** 1853